Master's thesis
Modeling Molecules and Nanosystems

Molecular Dynamics Simulation of Hypersound Attenuation in Thin Water Layers

Hilal Çomak

November 11, 2019

Supervisor: Antti Kuronen

Examiners: Antti Kuronen
Kai Nordlund

UNIVERSITY OF HELSINKI
Department of Physics
P.O. Box 64 (Gustaf Hällströmin katu 2a)
00014 University of Helsinki

HELSINGIN YLIOPISTO — HELSINGFORS UNIVERSITET — UNIVERSITY OF HELSINKI

Tiedekunta — Fakultet — Faculty	Laitos — Institution — Department
Faculty of Science	Department of Physics

Tekijä — Författare — Author
Hilal Çomak

Työn nimi — Arbetets titel — Title

Molecular Dynamics Simulation of Hypersound Attenuation in Thin Water Layers

Oppiaine — Läroämne — Subject
Modeling Molecules and Nanosystems

Työn laji — Arbetets art — Level	Aika — Datum — Month and year	Sivumäärä — Sidoantal — Number of pages
Master's thesis	November 11, 2019	64

Tiivistelmä — Referat — Abstract

Acoustic microscopy is a rising technology which uses phonons for obtaining images and measuring the mechanical properties of the samples. As opposed to other devices such as atomic force microscopy, light microscopy or X-ray spectroscopy, acoustic microscopy is non-invasive and can measure the subsurface of the material without any contact.

Commonly, water is used as a coupling medium in the acoustic microscope experiments of the biological samples. It is vital for the living organisms and necessary if one desires to conduct measurements while they are still alive. In order to improve the resolution of the images, we are interested in hypersound range of the phononic spectrum. However at this range, sound attenuation in water is one of the limitations. Sound attenuation is described as the decrease of the sound intensity, or loss of sound flux, during the propagation of sound through a medium. In most fluids, it increases with the square of the frequency. Consequently, there is a maximum frequency for a given distance between the lens and the sample and this affects the resolution.

In this thesis, we studied the hypersound attenuation in water with Molecular Dynamics Simulations. We used two different potentials mW and TIP4P/2005f for the simulations and we compared the results. In order to investigate the attenuation coefficient, we introduced varying sound signals with different frequencies 125 GHz, 250 GHz, 500 GHz, 750 GHz, 1 THz, 1.25 THz at the different amplitudes of 0.5 Å and 1 Å with both mW and TIP4P/2005f potentials and 0.25 Å with mW potential. We analysed the results by extracting the stresses from the simulation results and conducting Fast Fourier Transform Method for the signal content. Following, we obtained the Power Spectrum and plotted to observe how it changes with distance and calculated the attenuation coefficients for each cases.

The most obvious finding to emerge from this study is that at high frequency range, the sound signal attenuates in a couple of Å. Moreover, we observed that mW and TIP4P/2005f potentials give different results, but show similar trends. We also noticed some indications for a possible structural change and a stream.

Avainsanat — Nyckelord — Keywords
Molecular Dynamics, Nanoacoustics, Water Simulation

Säilytyspaikka — Förvaringsställe — Where deposited
University of Helsinki

Muita tietoja — övriga uppgifter — Additional information

Contents

1. Introduction

The concept of nanoscience and nanotechnology originates back to Richard Feynman's famous talk in 1959 titled "There's Plenty of Room at the Bottom: An Invitation to Enter a New field of Physics". In his talk, Feynman addressed the main problem and the art of this field: "manipulating and controlling things on a small scale" [1]. However, this manifesto-like talk was cited only few times in the following two decades [2]. Nanoscience could not be researched since it was difficult to probe the physics at that scale. After the invention of the scanning tunnel microscope [3] in 1981 and atomic force microscope [4] in 1986, nanoscience emerged as a rapidly advancing research field.

Today, developments in nanoscience have a direct impact on our everyday lives. These innovations are mostly founded on manipulation and control of electrons and photons. Their drastic effects can be experienced, for instance, in the improvement of semiconductor devices, lasers, wireless communication, optical fibres, microwaves [5], etc.

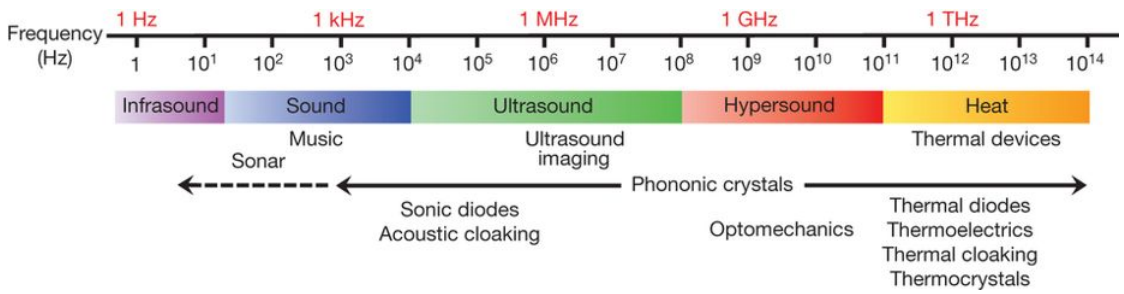

Figure 1.1: The phononic spectrum [5]

Another phenomenon which can be analysed and handled like electron and photon is the phonon. It is described as mechanical vibrations that exhibit sound and heat. Widely used applications of phononics at the kHz-MHz scale include ultrasound imaging, sonars, sonicators, and thermal imaging. However, other scales of the phononic spectrum (see Figure 1.1), especially nanoscale, just recently drew attention of scientists [6]. Manipulating and controlling phonons at the nanoscale provides another broad subfield with which one can introduce or improve new technologies, such as heat-assisted magnetic storage, thermoelectric conversion, phase-change data storage [7] or phononic metamaterials [8].

The acoustic microscope is one of the promising devices which uses phonons for obtaining images and measuring the mechanical properties of the samples. It is preferred over other devices such as the atomic force microscope, light microscope or X-ray spectroscopy due to its non-invasive measurements and the ability to gather information from within materials. What makes it different from other microscopes is the ability to examine the material under its surface and detect features.

However, this technique has several limitations such as attenuation and acoustic impedance. In the present work we will explore how sound attenuation behaves with high frequencies in a water medium using Molecular Dynamics (MD). To the best of our knowledge, there has not been relevant study reported previously in the literature with this method. We believe this to be of relevance for furthering the development of the acoustic microscope.

This study systematically examines the data for the attenuation coefficient of water, aiming to predict the effects of varying the frequency and amplitude of the applied signal. This thesis has been organised in the following way. Chapter 1 lays out the theoretical dimensions of the research, including phonons, sound in liquids, attenuation, generating sound at nanoscale, acoustic microscopy, and water as a coupling media. Chapter 2 presents the simulation method used for this

study. Chapter 3 provides the stress and spectral analysis of the simulation results. Following, it presents attenuation analysis and calculated attenuation coefficients. Chapter 4 contains conclusions on this work and discusses further research work.

1.1 Lattice vibrations and phonons

Phonons are quantized energy which are generated from the collective motion or vibration of atoms in a medium. Vibrations with small amplitude can be evaluated at the harmonic limit. In order to understand the basic idea of the vibration modes with wavelengths comparable to the lattice constant, one can use the simplistic system, a linear chain of atoms, representing a lattice [9].

In this model, a chain of identical atoms (see Figure 1.2) with an interatomic spacing (a) are connected by spring with a spring constant (K). We assume, that they can only move parallel to the chain, and there is a periodic boundary condition, so that each atom experiences the same environment.

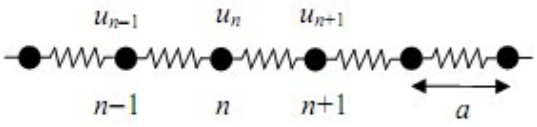

Figure 1.2: Linear chain with identical masses [10].

When force is applied to the atoms, they move from their equilibrium position with displacement (u_n). The equation of motion for this system and the total force on the n^{th} atom are written as:

$$M\,\frac{\partial^2 u_n}{\partial t^2} = -\frac{\partial E_p}{\partial u_n} = -K(2u_n - u_{n-1} - u_{n+1}). \tag{1.1}$$

If we try a plane wave solution:

$$u_n(t) = Ae^{i(kx_n^0 - \omega t)} = Ae^{i(kna - \omega t)}, \tag{1.2}$$

where $x_n^0 = na$ is the undisplaced position of the n^{th} atom. By substituting the solution in Equation 1.2 to the equation of motion (Equation 1.1), we obtain the dispersion relation:

$$M\omega^2 = 2K[1 - cos(ka)] \quad \Rightarrow \quad \omega = 2\sqrt{\frac{K}{M}\left|sin\Big(\frac{ka}{2}\Big)\right|} \tag{1.3}$$

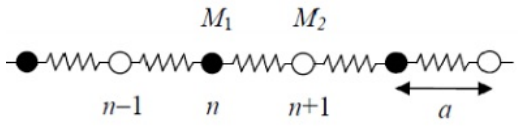

Figure 1.3: Linear chain with two atom types [10].

For the chain of two atom types with masses M and m, the dispersion relation is derived as the identical masses chain system and can be shown to have the form:

$$\omega^2 = \frac{K(m+M)}{Mm} \pm K\left[\left(\frac{M+m}{Mm}\right)^2 - \frac{4}{Mm}\, sin^2\left(\frac{1}{2}ka\right)\right]^{\frac{1}{2}} \tag{1.4}$$

We obtain two solutions for ω, upper and lower branch (see Figure 1.4). The lower branch is called acoustic branch, where the two types of atoms oscillate in-phase. The upper branch is called optical branch, where the oscillations of the two types of atoms are out of phase. They are both periodic in k vector with periodicity $2\pi/a$.

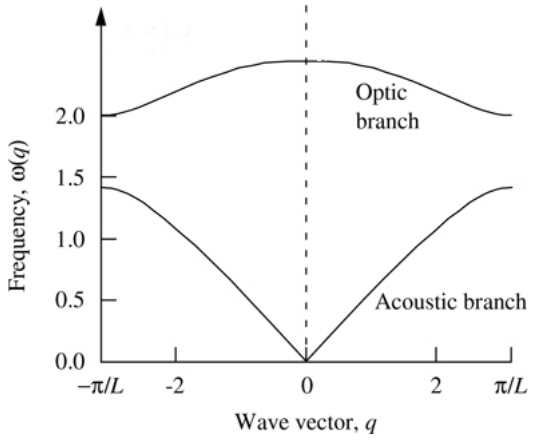

Figure 1.4: Dispersion relation of chain with two atom types [10].

As a generalization to a three-dimensional case, the wavenumber k is substituted by the three-dimensional wavevector $\mathbf{k}$. For the three-dimensional monatomic unit cell, there are three lattice modes, which are all acoustic. For the polyatomic unit cell with s different atoms, there are three acoustic branches (one longitudinal and two transversal) and $3(s-1)$ optical branches.

1.2 Sound in liquids

Liquids are defined as an intermediate phase between solid and gas. Like gas, it is classified as a fluid and is able to flow, on the other hand its density is closer to that of a solid than a gas. Due to its long particle displacements and strong intermolecular interactions, it is hard to predict behaviours of liquid with statistical mechanics [11].

Bolmatov and his colleagues [12] proposed a phonon theory in liquids and formalised a cut-off frequency. In their study, they revisit Frenkel's idea [13], which suggests a liquid relaxation time τ. It gives the time to recover from the stress and defined as the average time between two successive atomic displacement at one point in the liquid as illustrated in Figure 1.5.

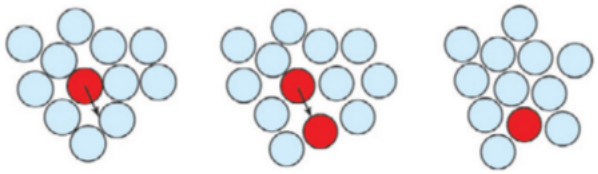

Figure 1.5: Illustration of a particle jump between two quasi-equilibrium positions in liquid [14].

It is known that sound in liquids travels as a longitudinal wave in which particles move parallel to the direction of the wave. According to Bolmatov's proposition, liquids also support shear waves when the frequency is larger than $1/\tau$, since the structure remains solid-like for times shorter than τ. By evaluating this idea and combining with Maxwell's relaxation time (see Equation 1.5), Bolmatov and his colleagues argue that liquids have transverse modes (support shear) with frequency $\omega > \omega_f$, where ω_f is Frenkel frequency. It is defined as [15]:

$$\tau = \eta/G \tag{1.5}$$

$$\omega_f = \frac{2\pi}{\tau(T)} = \frac{2\pi G_\infty}{\eta(T)}, \tag{1.6}$$

where η is the viscosity and G_∞ is the infinite frequency shear modulus. Transverse

dynamics is also validated by inelastic X-ray scattering experiments [16]. Moreover, a fast or second sound, which is an evidence of the transverse mode has been observed in some liquids by experiments [17] and simulation [18].

1.3 Sound attenuation

Sound attenuation is described as the diminishing of the sound intensity, or loss of sound flux, during the propagation of sound through a medium.

In metals, the main responsible mechanism for the sound attenuation is thermoelastic heat flow [19]. A longitudinal wave causes compression and rarefaction. Compression increases the temperature and heat flows from this region to a cooler spot, where rarefaction takes place, and this results in energy loss. In insulators, the main contribution arises from the damping of the sound wave due to the "phonon gas" and phonon-phonon collision in this phonon gas [20]. For semiconductors, the attenuation coefficient value is given between metals and insulators [21].

In liquids, the sound attenuation is not fully revealed. It can be divided in two broad categories:

- *Viscosity*: Because the medium is not ideal, there are thermal losses due to the viscosity. Stoke's law [22] gives the sound attenuation in Newtonian fluids, according to the fluid's viscosity.

$$\alpha = \frac{2\eta\omega^2}{3\rho V^3}, \tag{1.7}$$

  where η is the dynamic viscosity coefficient of the fluid, ω is the angular frequency of the sound, ρ is the fluid density, and V is the speed of sound in the fluid. As a result, the amplitude of the sound signal decreases exponentially along the distance with a rate α [23]:

$$P(x + \Delta x) = P_x e^{-\alpha(\omega)\Delta x}. \tag{1.8}$$

Viscosity is temperature and pressure sensitive so our attenuation due to viscosity will also be as well. Moreover, viscosity is dependent on the relaxation time τ as we mentioned in the previous section (see Equation 1.5).

- *Scattering*: The opposing behaviour that the material possesses to the acoustic pressure is defined as the acoustic impedance. It is the ratio between the acoustic pressure and the particle velocity in the sound wave [24]. Acoustic impedance is an important parameter to determine the transmit of the acoustic energy between two media. If the impedance mismatch is high, it is easier to observe the reflection and scattering [25]. Due to the boundary conditions at the interface of the two media, longitudinal wave motion is distorted with a viscous flow or a shear deformation. With molecular collision and friction, the viscous flow is converted to heat and attenuation takes place. This is commonly observed in non-homogeneous materials, such as porous and fibrous materials and materials with cavities.

1.4 Generating and detecting sound at the nanoscale

As mentioned in the Section 1.1, in order to create phonons one needs to introduce to the lattice a disturbance with an external source such as a sound transducer or a thermal excitation of the lattice. For the last 20 years, scientists use the picosecond or femtosecond lasers to generate the GHz-THz coherent phonons. It enables us to analyse the characteristics of the behaviour with high resolution and also gives an idea about its dynamics.

When a high frequency optical pulse excites the surface of a sample, part of the optical energy is absorbed (see Figure 1.6.1). This pulse is called *pump*. The generation of coherent acoustic phonons by the absorbed optical energy is explained with four microscopic mechanisms [26]. The most well known mechanism is *thermoe-*

lasticity. When a laser is incident upon a sample, resulting in heating, the sample's lattice vibration increases with the rise in temperature. At the anharmonic regime, thermal expansion takes place and causes strain in the lattice. Another mechanism is the *deformation potential*, which is caused by the modification of the electronic distribution. When incoming photons disturb the electronic distribution, interatomic interactions are modified accordingly, and this imposes strain and change in the lattice structure. *Inverse piezoelectric process* is another mechanism, in which the strain in the lattice is created with the macroscopic polarization induced by an electric field. During this process, electron heating and relaxation process cause time delay. The last mechanism is *electrostriction*, which is caused again by a weak electrical field. Since it deforms the orbitals, the dielectric constant and the density of the system and the electromagnetic density of energy are modified and this process creates strain.

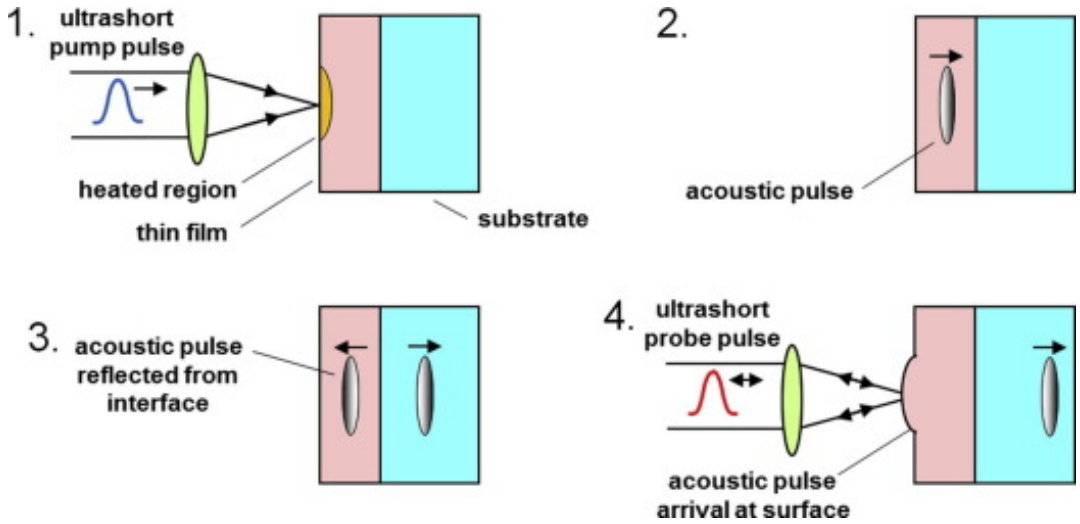

Figure 1.6: Illustration of a picosecond laser ultrasonics [27] 1) After an optical pulse excites the surface of a sample, part of the optical energy is absorbed and strain is created in the sample. 2) Due to the created strain, acoustic pulse propagates through the thin film. 3)At the interface, acoustic pulse is partially reflected back due to the acoustic impedance. 4) It is detected by the probe.

Due to the created strain, the acoustic pulse propagates through the thin

film and into the substrate (see Figure 1.6.2). At the interface, acoustic pulse is partially reflected back to the surface of the thin film due to the acoustic impedance mismatch (see Figure 1.6.3). Then it is detected by a second light pulse, which is called a *probe* (see Figure 1.6.4). By changing the time delay between pump and probe, one can measure the probe beam reflectivity or phase change and characterize materials [27]. With this technique, one can measure thermal conductivity and thin film thickness [28], carrier diffusion in semiconductors [29] and electron diffusion in metals [30], mechanical properties [31, 32] and study vibrational modes [33].

1.5 Acoustic microscope

Acoustic microscope experiments have been conducted since 1959, however the frequency range was limited only up to a few GHz [34]. With the development of the picosecond lasers, it has been possible to measure at higher frequencies, which provides a better resolution in the range of micrometer [35] to nanometer [36].

Some characterization experiments in cell biology are designed with atomic force microscopy [37], X-ray reflectometry [38], optical and vibrational spectroscopy [39]. Nonetheless, in these experiments, either external stress is applied via contact or applied excitation causes damage or ionization in the sample [40]. However with acoustic microscopy, one can measure mechanical properties without contact and damage [41]. Moreover, in contrast to light microscope, with greater penetration depth, it provides information about the sub-surface [42]. Additionally, it enables us to perform measurements on living organisms at micro-nanoscale in a time span and detect their dynamical properties (Figure 1.7b) by taking snapshots.

A schematic diagram of an acoustic microscope is shown in Figure 1.7a. In this set-up, a short light pulse is absorbed by the thin aluminium film and strain propagates through an optical cavity. It is reported that the optical cavity is placed to increase the absorption of the pump light and therefore the amplitude of the

produced sound [43]. Generated sound is focused with the concave acoustic lens and passes through liquid coupling medium (water in our case) and reflects from the surface of the sample. This causes a change in the cavity spacing, as a result, the reflectivity of the probe light alters and the change is measured.

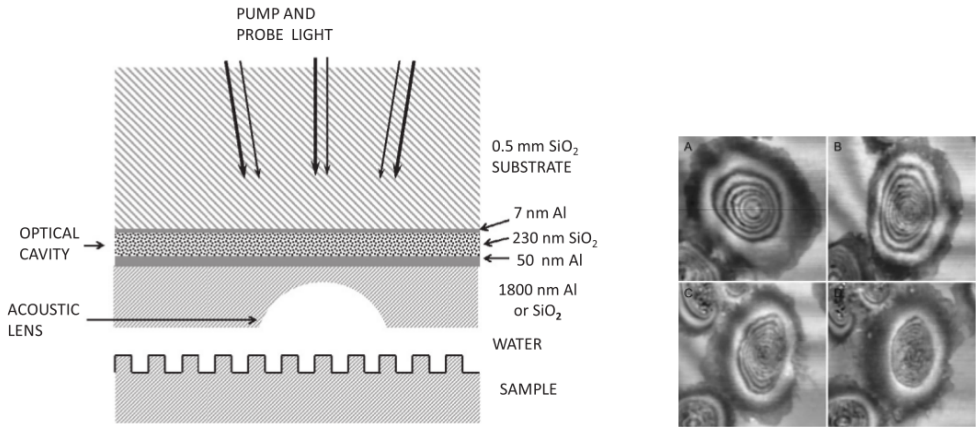

(a) **(b)**

Figure 1.7: a) Schematic diagram of the opto-acoustic microscope [35]. b) Acoustic image of a HaCaT cell. Figure 1.7b A and B are taken before, Figure 1.7b C and D after the drug application [44].

One of the limitations of this technique is the reduction of the sound power across the interfaces. Due to the acoustic impedance mismatch of different media, at the boundary sound signal is reflected back partially. For example, aluminium and water have an impedance ratio of $Z_1/Z_2 = 11.7$ and it reduces the amplitude of the signal by a factor 0.29 [35].

Another limiting factor is the attenuation in the coupling medium. Attenuation of sound in liquids is proportional to the square of the frequency of the signal (see Section 1.3). Thus, there is a maximum frequency for a given distance between the lens and the sample and the limitation of the frequency directly affects the resolution of the obtained image. In a study conducted in 1977, the attenuation coefficient per distance for low frequencies is given as $\alpha = \beta f^2$, where β is 19 x $10^{-17} s^2 cm^{-1}$ and f is the frequency at 30 C°[35, 45]. Data for the attenua-

tion coefficient at high frequencies are measured with Brillouin Spectroscopy [46] and Inelastic X-ray Scattering[47]. Erokhin [46] summarized these results as in the Figure 1.8 below.

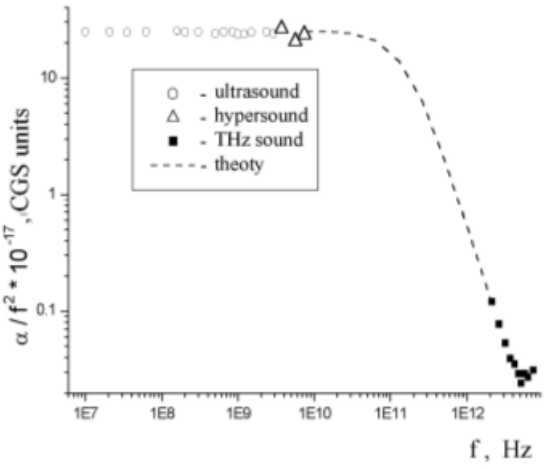

Figure 1.8: Sound attenuation in water [46].

Other than water, one can also use other coupling media such as olive oil, glycerol or methanol. However, water is a particularly common choice. In the section that follows, we will explain the importance of the water as coupling medium for the acoustic microscopes.

1.6 Water as a coupling medium

Mechanical properties of cells and inner organelles like the nucleus or cytoplasm have important roles during some of the biological processes such as migration, differentiation, proliferation [48]. For example, mechanical forces on the cell surface or the receptors propagate through the cytoplasm and focus on the nucleus or a certain focal point in cytoplasm and this applied force affects the chemistry and therefore the gene activity in the nucleus [49]. It has been also speculated that the changes in mechanical properties of the nucleus, cell, and its microenvironment are important to reveal the progression pathways of some diseases such as cancer [50], Alzheimer,

Parkinson, in the sense of feeling other cells or the environment stiffness [51]. However, their mechanical properties during these processes are not clear. At this point, the acoustic microscope provides the opportunity to measure the mechanical properties of the living organisms non-invasively during these processes.

If one desires to observe the properties of living organisms, it is necessary to do the measurements in an environment that can sustain life, which water fulfills for these organisms of interest. Around 70 % of the total cell mass is water [52]. It plays a role in many biological processes such as protein folding [53], protein binding [54] and molecular recognition [55].

1.7 Water

Water is a simple molecule, yet it has anomalous properties due to its structure. Two hydrogen atoms are bonded to an oxygen atoms with covalent bonds (see Figure 1.9a). Due to the electronegativity difference between the hydrogen and oxygen atoms, there exists a net dipole moment pointing from oxygen to the center of two hydrogen atoms. The average length of the covalent bond between oxygen and hydrogen atom is 0.95721 Å and the angle between these bonds is 104.5 °. Arising from the partial charge difference between oxygen and hydrogen atoms, hydrogen bonds (O-H bond) are formed between the negative side of the molecule and the positive side of the other water molecule [56]. Formed hydrogen bonds are responsible for the peculiar behaviours such as different crystal structures (see Figure 1.9b) depending on temperature and pressure.

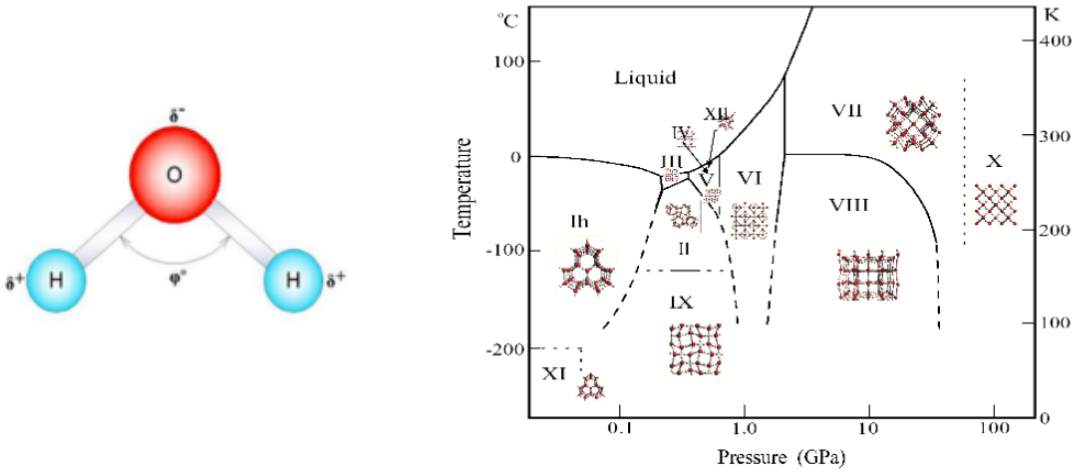

(a) **(b)**

Figure 1.9: a) Ball and stick model of a water molecule with the angle 104.5°between oxygen and hydrogen atoms [56]. b) Different crystal structures depending on temperature and pressure [57].

2. Methods

In this chapter, we will introduce the simulation and analysis methods, that we used. In Section 2.1, we will discuss why Molecular Dynamics is necessary for this study. In Section 2.2 we will explain the algorithm of the Molecular Dynamics and the used timestep, temperature and pressure control. We will continue with an overview of different interatomic potentials for water and explain mW and TIP4P/2005f potentials in more detail. In Section 2.3, we will present our simulation details. In Section 2.4 and Section 2.5, we will briefly explain the calculation of stress with the atomistic method and Fast Fourier Transform method, respectively.

2.1 Why Molecular Dynamics?

There are some studies of acoustics with other simulation methods, such as Finite Element Method [58] that is implemented in e.g. in COMSOL [59]. However, since we aim to investigate the acoustic mechanisms at the nanoscale, we will use Molecular Dynamics. In our study, acoustic excitation varies in the hypersound range, whose wavelength range (10^{-9}m - 10^{-12}m) is close to the molecular spacings (1.97 Å for water). At this regime, structural change might take place and contiuum flow is not a good approximation as stated with Knudsen number [60]. Hence, an analysis at the nanoscale with Molecular Dynamics is crucial for this study.

Previously, MD was not a viable analysis method for acoustics due to the computational complexity. However, with the increasing availability of computational

resources in supercomputers as well as the advances in calculation techniques, we have enough resources to simulate nano sized systems at the atomistic scale. This provides us means to investigate the phenomena at the nanoscale which are different from the microscale.

This change not only affected acoustics but also allowed for the bridging of acoustics with other research fields in nanosicence such as sono-chemistry [61], sono-luminescence [62], metamaterials [63], and defect manipulation in materials [64].

2.2 Molecular Dynamics

Molecular Dynamics is a simulation method used to calculate the equilibrium and dynamic properties of systems at the atomistic level [65]. It was developed by Alder and Wainwright in 1957 [66]. MD simulations connect the microscopic and macroscopic scale with the Ergodic Hypothesis, which asserts, that the time average of a system is equal to the ensemble average [67]. This makes MD a useful tool to link experiments with theory. It has many applications in material science, atmospheric science, biophysics, biochemistry and medicine.

2.2.1 Algorithm

The essential idea of MD is determining the trajectories of constituent particles at each step. The velocity and the position of the particles are calculated by solving the Newton's equations of motion numerically. In classical MD, based on the Born-Oppenheimer approximation, electrons and nuclei are treated separately due to their mass difference [68]. It is assumed that electrons move faster than nuclei and reach the equilibrium configuration immediately. Therefore, they do not take part in the classical MD calculations, however, they are taken into consideration in the interatomic potential.

Figure 2.1 presents a basic flowchart of the MD algorithm. As the first step, positions of the particles r_i are set with the desired configuration. Initial velocities v_i are given accordingly to a Gaussian Distribution.

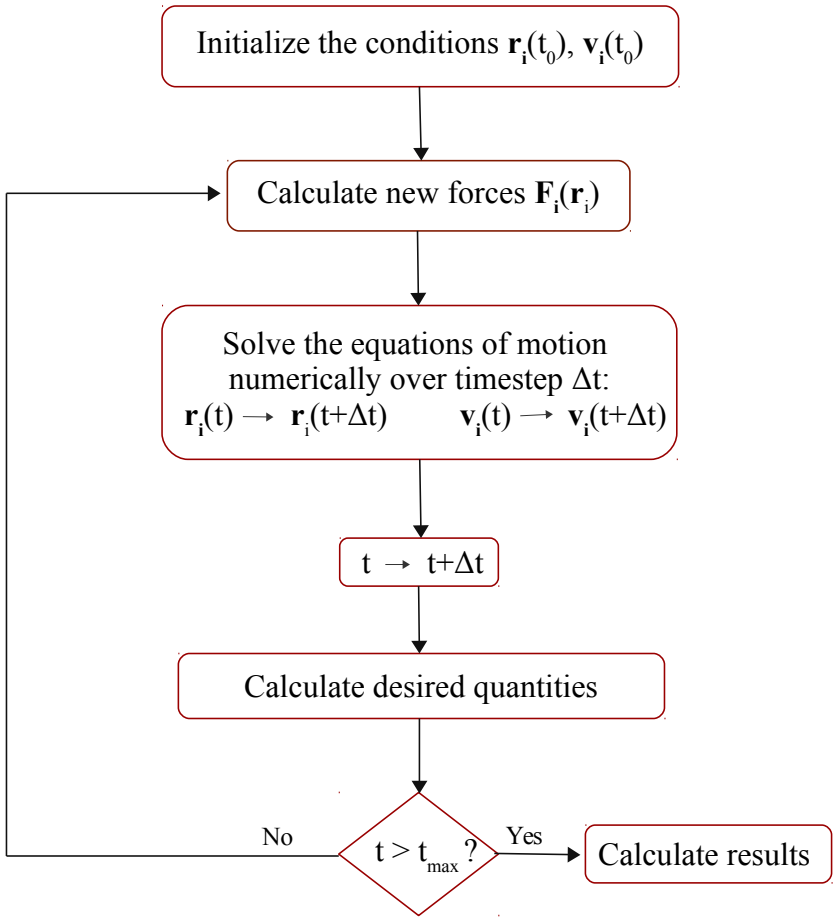

Figure 2.1: A basic flowchart of the MD algorithm [69].

Atomic forces are derived from the potential functions $U(r_1, r_2, ...r_N)$, which are determined according to the geometric arrangement of particles,

$$\mathbf{F}_i(r_1, r_2, ...r_N) = -\nabla_{\mathbf{r}_i} U(r_1, r_2, ...r_N). \tag{2.1}$$

If there is no external force, the two-body potential energy can be written as:

$$U = \sum_{i=1}^{N} \sum_{j>i}^{N} u(r_{ij}), \tag{2.2}$$

where $r_{ij} = |r_i - r_j|$. The requirement $j > i$ avoids counting the pairs twice and this helps to reduce the computational expense arising from solving the equation of motion which is proportional to N^2 for N particles. An additional way to decrease the computational expense is defining a cut-off radius, where for particle separation distances beyond the cut-off ($r_{ij} > r_{cut-off}$) the potential energy between the particles is 0. The chosen cut-off should be smaller than half the box side length, in order to avoid the possible interaction between the particle and its replica with the periodic boundary condition (pbc) [65]. With pbc, the simulation box is replicated in each direction, so that particles experience forces as they are in a bulk system.

After calculating the total force on each particles, simulation continues with solving Newton's equation of motion iteratively with an integrator.

$$m\frac{d^2\mathbf{r}_i}{dt^2} = \mathbf{F}_i(r_1, r_2, ...r_N) \qquad i = 1, 2, ...N \tag{2.3}$$

In this study, all simulations were conducted with the MD simulator LAMMPS (Large-scale Atomic / Molecular Massively Parallel Simulator) [70], in which Velocity Verlet [71] was implemented. Verlet Algorithm [72] is widely preferred in MD, since it is simple, reversible in time and it conserves energy and momentum [73]. Velocity Verlet is a modified version of Verlet Algorithm which enables the update of the velocity and positions simultaneously. At each time step Δt, the next position $r(t + \Delta t)$ and velocity $v(t + \Delta t)$ of the particles are calculated from the current positions $r(t)$ and accelerations $a(t)$ obtained from Newton's equation of motion and the previous positions $r(t - \Delta t)$ [74],

$$r(t + \Delta t) = r(t) + \Delta t\, v(t) + \frac{\Delta t^2 a(t)}{2}, \tag{2.4}$$

$$v(t + \Delta t) = v(t) + \frac{a(t + \Delta t) + a(t)}{2}\, \Delta t. \tag{2.5}$$

One drawback of this algorithm might be the precision loss of the position during the approximation with Taylor's expansion and derivation of the velocity from it.

Another modified version of Verlet Algorithm, Leapfrog Method [75] and Gear5 predictor-corrector algorithm [76] can be named as other prevalent integrators.

2.2.2 Timestep

Choosing a correct time step has a critical role in the integration algorithm. If the time step is too short, the number of the iterations needs to be large so that the computation is able to finish at the desired time, which increases the computational cost. On the other hand, when a longer time step is chosen, the accuracy of finding the "correct trajectory" of the particles decreases. Aside from this trade-off, it is recommended to assign time step approximately one order of magnitude smaller than the shortest motion in the system [74]. For instance, the suggested time step for flexible molecules with flexible bonds is around 0.1 fs [77].

2.2.3 Temperature and pressure control

In LAMMPS, temperature and pressure control are performed with the Nosé-Hoover method. Nosé introduced a 'time scaling' factor to the Hamiltonian, which adjusts the kinetic energy with feedback [78] . Hoover developed this method by adding a time-dependent fictitious parameter which behaves like friction and changes the acceleration [79]. The extended Hamiltonian is given as:

$$H = \sum \frac{|p_i|^2}{2m} + U(r^N) + \frac{\xi^2 Q}{2} + 3Nk_BTln(s), \tag{2.6}$$

where H is the energy of the N body system, p is the momentum, m is the particle mass, U is the potential energy between particles, ξ is the pseudofriction coefficient, Q is the heat bath mass, k_B is the Boltzman constant, T is the temperature and s is the scaling factor.

The time evolution of the position and velocity is implemented using the system

of coupled differential equations:

$$\frac{d\mathbf{r_i}}{d_t} = \mathbf{v_i}, \tag{2.7}$$

$$\frac{d\mathbf{v_i}}{dt} = -\frac{1}{m_i}\frac{\partial U r^N}{\partial \mathbf{r_i}} - \xi\, \mathbf{v_i}, \tag{2.8}$$

$$\frac{d\xi}{dt} = \frac{\sum m_i |\mathbf{v_i}|^2 - 3Nk_BT}{Q}, \tag{2.9}$$

$$\frac{d\, lns}{dt} = \xi. \tag{2.10}$$

The scaled position and velocity are coupled with the Velocity Verlet Algorithm. The pseudofriction variable ξ should be chosen carefully, so that the energy fluctuations agree with the canonical ensemble. If the pseudofriction variable ξ is positive, energy is taken from the system; if it is negative, the energy is deposited to the system. Choosing a correct heat bath mass Q is important to determine the thermostat effectiveness, since it provides the coupling between the heat bath reservoir and the physical system. Too small of a mass causes high frequency oscillations, on the other hand, mass values which are too large, might result in a long simulation time to reach the desired temperature or pressure.

Nosé-Hoover method is also used in pressure control by rescaling the simulation box dimensions, particle position and momenta. However, they need to be adjusted separately, since the particle positions and momenta change faster than the volume [80]. Other popular techniques to control the temperature and pressure are Berendsen Thermostat/Barostat [81] and the Andersen Thermostat/Barostat [82].

2.2.4 Interatomic potentials

The interatomic potential plays an important role in the MD simulations, since the results of the calculations are directly connected to the atomic forces, which are obtained from the interatomic potential (see Equation 2.1). Developing a precise water potential model, which fulfils the thermodynamic conditions and predicts

the microscopic environment is a continuing research, since the introduction of the Molecular Dynamics simulations method [83].

Generally, each water molecule is defined by three or more interaction points and can be modified according to the desired properties such as the rigidity, flexibility and polarizability [84]. *Rigid* models possess fixed molecular geometry and only intermolecular interaction are taken into account. *Flexibility* is introduced by harmonic or anharmonic potential functions for the intramolecular interactions, which enables bond stretching and angle bending. As a result, the geometry of the water molecule changes with the environment conditions. *Polarizability* is introduced as an explicit term, which implements the redistribution of the charge due to the applied electric field.

In 2002, Guillot [85] reported that there have been 46 water models proposed. However, none of them is fully satisfactory in terms of predicting all behaviours, since they are developed for the specific purposes. Atomistic water models differ from each other by [56, 86]:

- *The charge distribution*: Positive charges are on the H atoms but the negative charges are placed differently. For example, Transferable Intermolecular Potentials (see Figure 2.2), for three interaction with three interaction points (TIP3P) [87], with four interaction points (TIP4P) [87], with five interaction points (TIP5P) [88] and Simple Point Charge Model (SPC) [89] can be named as the most common rigid models.

  In TIP3P model, each atom has a point charge (see Figure 2.2.a). TIP4P has a fictitious negative charge located on a dummy particle M, to be able to change the center of negative charges and improve the electrostatic distribution (see Figure 2.2.b). TIP5P contains 2 partial charges on the lone pairs sites of the oxygen in addition to charges on the oxygen and hydrogen (see Figure 2.2.c). SPC is very similar to the TIP3P with respect of the location of the charges

on hydrogen and oxygen atoms, however it is differently parametrized.

- *The bond geometry*: Bond length and the H-O-H angle vary depending on the proposed model. For instance, in most rigid models, the H-O-H angle is 104.5°, as the experimental value, however SPC possesses an H-O-H angle of 109.47°.

- *The parametrization*: Parameters of the interatomic potential model are fitted to reproduce the available experimental values of the desired thermodynamic property.

- *Internal degrees of freedom*: In some models such as TIP4P/2005f, O-H bond stretching (TIP4P/2005f and SPC/E) and H-O-H angle bending are included.

- *Non-additive interaction terms*: Polarization, charge redistribution, three-body and higher order interaction are introduced. For example, in order to predict the dipole moment and the dielectric constant of water, polarization is included as in the GCPM [90] potential model. This term enables to redistribute the charge due to the applied electric field.

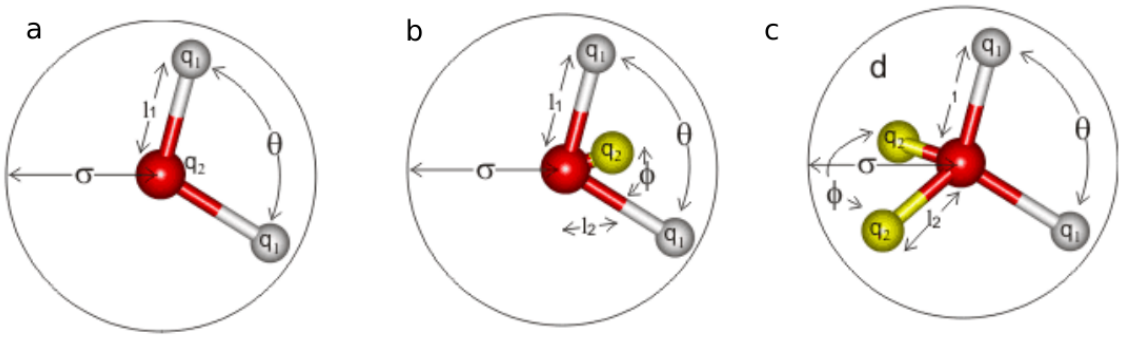

Figure 2.2: Schematic water models with a) three b) four c) five interaction points [91].

Here, in this thesis, we started to test the simulation parameters with mW, due to its computation time and simplicity. Later on, we simulated with TIP4P/2005f,

since it is the most realistic potential despite of its downsides such as long computing time or undesirable narrowing in H-O-H angle [85].

mW water model

When the simulation system consists of large number of water molecules and the simulation requires a long time, the computational costs get very high. In order to overcome the time and size limitations, coarse-grained molecular (CG) model of water has been introduced. In the CG model of water, one or more water molecules are represented by a "superatom" which reduces the degree of freedom and "acts as a collective entity" [92].

Molinero proposed the monatomic coarse-grained model for water (mW) with tetrahedral structure [93]. The tetrahedral structure of water is a result of hydrogen bonds (short-ranged interaction), which are caused by (long-ranged) electrostatic interactions. In this regard, instead of taking the electrostatics into account as it is in classical atomistic models, in the mW coarse-grained model the tetrahedral structure is described by using only the short-ranged interactions and excluding hydrogen atoms. With the resemblance of water and silicon in their tetrahedral

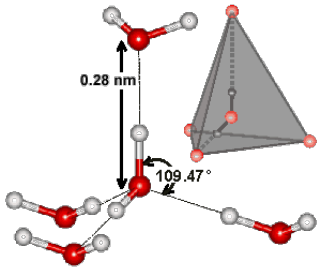

Figure 2.3: Schematic drawing of tetrahedral structure of water molecules [93].

structure, phase diagram and anomalies, the Stillinger-Weber (SW) potential is taken as a basis and the parameters for the water are fitted. The SW potential was originally proposed for the Si-Si interaction, which consists of a pairwise interaction and three body term, adjusting the tetrahedrality. The SW potential as a function

of distance between pairs of atoms and angles between triplets atoms is written as [93]:

$$E = \sum_i \sum_{j>i} \varphi_2(r_{ij}) + \sum_i \sum_{j\neq i} \sum_{k>j} \varphi_3(r_{ij}, r_{ik}, \theta_{ijk}), \tag{2.11}$$

$$\varphi_2(r) = A\varepsilon \left[B \left(\frac{\sigma}{r}\right)^p - \left(\frac{\sigma}{r}\right)^q \right] exp\left(\frac{\sigma}{r - a\sigma}\right), \tag{2.12}$$

$$\varphi_3(r, s, \theta) = \lambda\varepsilon \left[cos\theta - cos\theta_0\right]^2 exp\left(\frac{\gamma\sigma}{r - a\sigma}\right) exp\left(\frac{\gamma\sigma}{s - a\sigma}\right), \tag{2.13}$$

where A, B, p, q and γ scale the potential, a is the reduced cutoff, where at a distance $a\sigma$, the potential and forces go to zero, cosine of the θ, provides the tetrahedral angle, λ scales the strength of the tetrahedral interaction and the repulsive three-body term, ε gives the the depth of the pairwise interaction potential for the energy scale and σ is the particle diameter. The values for parameters for water are presented in the Table 2.1.

Table 2.1: Parameters used in mW potential for water [93].

A	B	p	q	γ	a	ε (kJ/mol)	λ	σ (Å)
7.049556277	0.6022245584	4	0	1.2	1.8	25.895	23.15	2.3925

TIP4P/2005f water model

Rigid models (for eg. TIP4P, TIP3P, SPC) are simple and they can produce many good results. Yet they prohibit molecules from adapting to their environment, since they do not allow changing the geometry and charge distribution of the molecules. Therefore, certain properties like self-diffusion constant, dielectric constant and dipole moment, which are dependent on the external factors, can not be calculated effectively. In order to overcome this obstacle, a flexible model, TIP4P/2005f [77] was introduced. This model adjoins the bond stretching and angle bending to the rigid model TIP4P/2005 [94].

In TIP4P/2005f, there are 4 interaction sites as in other TIP4P-like models (see Figure 2.2.b). Three of them are located on the oxygen and hydrogen atoms. The other interaction site is a fictitious point M-site, which is placed at the same plane of the O and H atoms and at the bisector of the H-O-H angle. The purpose of adding a fictitious point M is to improve the model by modifying the charge distribution around the oxygen atom [95]. Since TIP4P/2005f is not a rigid model, the position of the fictitious point M, d_{OM}, is determined with respect to the locations of hydrogen atoms such as:

$$z_{OH_i} = d_{OH}\, cos(\theta/2), \tag{2.14}$$

$$d_{OM} = d_{OM}^{\text{rel}}(z_{OH_1} + z_{OH_2}), \tag{2.15}$$

where d_{OH} is the distance of hydrogen atom to the oxygen and θ is the H-O-H angle. The parameter d_{OM}^{rel} is chosen so that it gives d_{OM} of the TIP4P/2005 model (with the parameters $d_{OH} = 0.9572$, $\theta = 104.52$, $d_{OM}^{rel} = 0.13194$, hence $d_{OM} = 0.1546$).

The intramolecular potential is written as the sum of the O-H bond stretching and H-O-H angle bending:

$$V^{intra} = V_{OH_1} + V_{OH_2} + V_{HOH}(\theta). \tag{2.16}$$

Flexibility to the O-H bond is introduced with the Morse potential, which is defined as:

$$V_{OH_i} = D_r \left\{1 - exp\left[-\beta\left(r_{OH_i} - r_{\text{eq}}\right)\right]\right\}^2, \tag{2.17}$$

where r_{eq} is the bond length at the equilibrium, r_{OH_i} is the instantaneous bond length, D_r determines the strength of the bond and β is a Morse potential parameter, which gives the width. The Morse potential is an anharmonic function, which allows the bond breaking and gives better results than the harmonic function for the molecular vibrational spectra [96].

Contribution of the angle bending is calculated with the harmonic function, which is written as:

$$V_{HOH}(\theta) = \frac{1}{2}\, K_\theta \left(\theta - \theta_{\text{eq}}\right)^2. \tag{2.18}$$

Parameters for the molecular geometry at equilibrium differ from the TIP4P/2005 model and the experimental results. In this model, flexibility causes O-H bond elongation and H-O-H angle narrowing. Therefore, the angle at the equilibrium ($\theta_{\text{eq}} = 107.4°$) is larger and the bond length at the equilibrium ($r_{\text{eq}} = 0.9419$Å) is shorter than experimental values.

The intermolecular potential is based on the Lennard-Jones interaction potential U_{LJ} and electrostatic Coulomb potential $U_{\text{electrostatic}}$ as in rigid models. The Lennard-Jones potential is calculated between two neutral oxygen atoms of two molecules by including the repulsive and attractive forces caused by the electron cloud overlaps and induced dipoles, respectively [97]. It is calculated as:

$$U_{LJ} = 4\epsilon \left[\left(\frac{\sigma}{R_{\text{OO}}} \right)^{12} - \left(\frac{\sigma}{R_{\text{OO}}} \right)^{6} \right], \tag{2.19}$$

where ϵ is the measurement of the strength of the attractive force between particles, σ is the minimum distance where two non-bonded particles get together and R_{OO} is the distance between two neighbouring oxygen atoms.

The electrostatic interaction is calculated between two positive charges placed at the hydrogen atoms and the fictitious negative charge on M-site. It is formulated as:

$$u_{\text{electrostatic}} = \frac{e^2}{4\pi\epsilon_0} \sum_{a,b} \frac{q_a q_b}{r_{ab}}, \tag{2.20}$$

where e is the proton charge, ϵ_0 is the permittivity of vacuum, q_a and q_b are the electric charges at the charged sides of two different molecules. The potential parameters can be found in the Table 2.2 below:

Table 2.2: Parameters used in TIP4P/2005f [77].

ϵ/k (K)	σ (Å)	q_H (e)	q_O (e)	q_M (e)	d_{OM}^{rel} (Å)	D_r (kJ/mol)	r_{eq} (Å)	β (nm^{-1})	θ_{eq} (°)	K_θ (kJ/mol rad^2)
93.2	3.1644	0.5564	0	$-2q_H$	0.13194	432.581	0.9419	22.87	107.4	367.810

2.3 Simulated system details

In this work, the attenuation of hypersound in water was simulated by introducing a Gaussian wave packet with varying frequencies and amplitudes for both the mW and TIP4P/2005f potentials.

We started by creating simulation boxes. For the simulations with mW potential, a box with 320 Å each side length was built by using LAMMPS MD Simulator. The number of the molecules was calculated according to the box size, so that the density of the system is 1 g/cm^3. 1095355 mW water molecules were created and randomly distributed.

Compared to the mW potential, for the simulation with TIP4P/2005f potential, O and H atoms, dummy electronic charges and the OH bond vibration are taken into calculation separately as mentioned in Section 2.2.4, thus the required computation time increases. Therefore, in order to reduce the computation cost, we decided to build a smaller (half of mW) simulation box with dimensions $x = 320$ Å , $y = 320$ Å and $z = 160$ Å for the simulation with TIP4P/2005f potential. With a script, 500000 water molecules were created with the proper bond length and angle according to the TIP4P/2005f potential parameters with a cubic lattice as an initial structure.

For both systems, the velocities of atoms were assigned using the Gaussian distribution. The periodic boundary condition was applied in all directions. The system was equilibrated by using NPT ensemble at 300 K and 1 atm.

The timestep for mW was 1 fs and the total equilibration time was 1 ns. The timestep for TIP4P-2005f was chosen as 0.2 fs, which is close to the recommended value [77], and the system was equilibrated for 1.2 ns.

An oscillating wall formed by fixed water molecules (width = 10 Å) is located in the middle of the box as a sound source (see Figure 2.4). The excitation is introduced by oscillating the wall in the x direction, which generates a Gaussian

wave packet which has the form:

$$A = A_0 e^{-((t-t_0)^2)/2\sigma^2} \sin(2\pi f t), \tag{2.21}$$

where A is the amplitude of the packet, σ is the gaussian width, f is the frequency, and t is the time.

In order to analyse the attenuation of hypersound in water, we introduced different signals with frequencies 125 GHz, 250 GHz, 500 GHz, 750 GHz, 1 THz, 1.25 THz at the different amplitudes of 0.5 Å and 1 Å with both the mW and TIP4P/2005f potentials, and 0.25 Å with the mW potential.

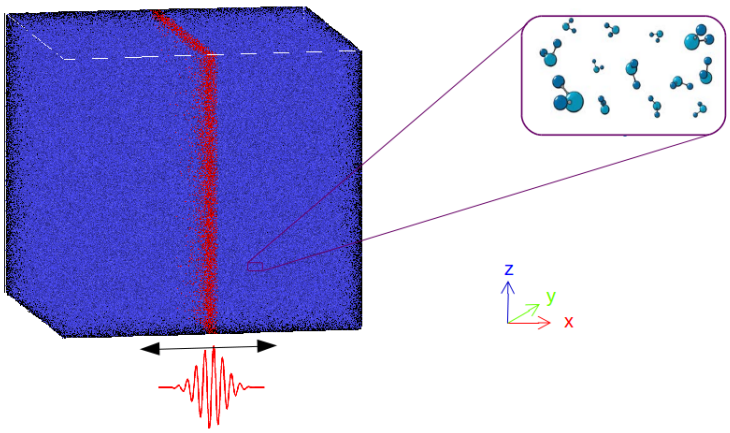

Figure 2.4: Simulation box.

2.4 Calculation of stress with the atomistic method

In order to investigate the attenuation of the signal, as the first step, the stress for the simulated system is calculated. The stress tensor for each atom is calculated by

LAMMPS with the formula below [98]:

$$S_{ab} = -\Bigg[mv_a v_b + \frac{1}{2}\sum_{n=1}^{N_p}(r_{1_a}F_{1_b} + r_{2_a}F_{2_b}) + \frac{1}{2}\sum_{n=1}^{N_b}(r_{1_a}F_{1_b} + r_{2_a}F_{2_b}) + \frac{1}{3}\sum_{n=1}^{N_a}(r_{1_a}F_{1_b} + r_{2_a}F_{2_b} + r_{3_a}F_{3_b}) + \frac{1}{4}\sum_{n=1}^{N_d}(r_{1_a}F_{1_b} + r_{2_a}F_{2_b} + r_{3_a}F_{3_b} + r_{4_a}F_{4_b}) + \frac{1}{4}\sum_{n=1}^{N_i}(r_{1_a}F_{1_b} + r_{2_a}F_{2_b} + r_{3_a}F_{3_b} + r_{4_a}F_{4_b}) + Kspace(r_{ia}, F_{ib})\Bigg].$$

The first term gives the kinetic energy of an atom. The second term is the pairwise energy of an atom with its neighbours, where n iterates to N_p, r_1 and r_2 are the positions of the pair atoms and the F_1 and F_2 are the forces forming by the pairwise interaction. Similarly, bond, angle, dihedral and improper interactions contributions are calculated as third, forth and fifth terms of the equation, respectively. Kspace contribution arising from the long Coulomb interactions is also added.

Obtained results were extracted with Ovito's Python interface *ovitos*, by allocating the molecules into bins and reducing the desired properties of the molecules within the bin. Here, we calculated stress profile along x axis to obtain stress tensor σ_{xx}, since we introduced the signal along the x axis.

2.5 Analysis with Fast Fourier Transform

In 1822, Joseph Fourier describes heat flow as a signal which is represented with a sum of sinusoids [99]:

$$x(t) = \sum_{n=1}^{\infty} A_n \sin(2\pi n f t + \phi_n). \tag{2.22}$$

In our study, to be able to analyse the content of the applied acoustic signal (see Equation 2.21) and how it varies through the distance, we applied Fast Fourier Transform (FFT) on the stress results. FFT is an efficient algorithm to convert a signal from the time-domain functions into the frequency-domain [100]. Based on the Fourier series, Fourier Transform equation is written as:

$$X(f) = F\{x(t)\} = \int_{-\infty}^{\infty} x(t)\, e^{-j2\pi f t} dt, \tag{2.23}$$

where $x(t)$ is the time domain signal, $X(f)$ is the FFT, and $f(t)$ is the frequency to analyse.

After we obtained the frequency composition, in order to obtain power of the frequency components, we squared the magnitude of the frequency peaks, which is also proportional to the intensity.

3. Results and discussion

In this chapter, we will present the calculated results and discuss them. In Section 3.1 we will first analyse the stress results. In Section 3.2, we will focus on the FFT results. In Section 3.3 we will show acoustic attenuation results of all simulations. Following, in Section 3.4 we will show the attenuation coefficient results obtained from the previous sections.

3.1 Stress analysis

We start the analysis with the stress evaluation to have an initial idea about how the simulation behaves. For this section, we only show examples for the representative cases.

3.1.1 Stress analysis of the simulations with mW potential

Figures 3.1a and 3.1b present the calculated stress as a result of the applied force by the introduced signal. We obtained stress as explained in the Section 2.4 and created surface plots (Figure 3.1). Figure 3.1a shows the 3D plot from another viewpoint.

The y-axis gives the time which is printed every 50th timestep. Colour coding of the plots gives the calculated stress (z-axis) of the atoms in each bin (x-axis). The blue block, which can be seen in the middle of the surface plots represents the fixed atoms in the simulation.

In Figure 3.1a, exponentially decaying peaks reveal the attenuation of the sig-

nal. What is striking about this figure is that our simulation box is not big enough to avoid the periodic boundary condition effects. At two sides of the plot, in Figure 3.1a, we can observe the bumps, which are caused by the particles pushed by the signal from the other side of the simulation box. Due to the computational capacity limitations, we did not simulate with a bigger simulation box. However, we will consider this effect in the further analysis.

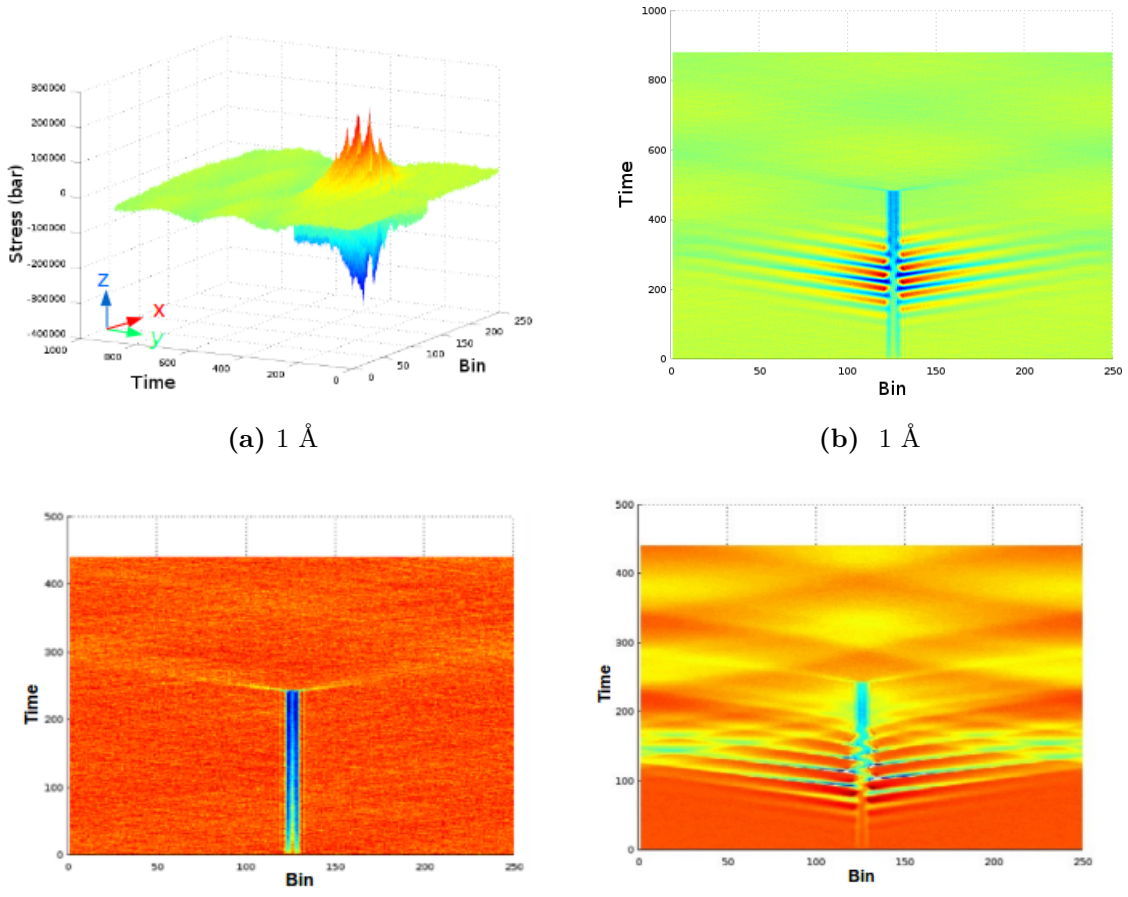

(a) 1 Å **(b)** 1 Å

(c) 0.01 Å **(d)** 5 Å

Figure 3.1: Stress profiles of the mW simulation systems with different amplitude. Figure 3.1a shows the three dimensional surface plot. Figure 3.1b, 3.1c and 3.1d present the plot in two dimension view. Variables are frequency $f = 500$ GHz with Gaussian width $\sigma = 3000$ fs and amplitudes A_0 a) 1Å b) 1Å c) 0.01Å d) 5Å.

Additionally, stress plots were useful to determine the reasonable amplitude for the simulations. For example, as it can be seen in Figure 3.1c, a signal with the amplitude 0.01Å is not big enough to beat out the thermal noise. Another example is a signal with high amplitude 5Å, which can be seen in the Figure 3.1d. In this case, due to the periodic boundary condition, the signal interferes with the reflected wave from the boundary and this prevents us to analyse the attenuation of the signal. Furthermore, high amplitude might take us in the anharmonic region, which we try to avoid (or which is undesired) in this study. The next section of the analysis is the FFT of the calculated stress.

3.1.2 Stress analysis of the simulations with TIP4P/2005f potential

Figures 3.2a and 3.2b present the stress profiles of a simulation with the TIP4P/2005f potential. We used TIP4P/2005f potential with the same inputs for the signal as in mW so they would be comparable. When we compare the stress profile with mW's, we can see that the intensities of sound signal in the simulations are not the same. We can find a possible explanation by considering the main difference between two potentials. In contrast to mW, with TIP4P/2005f, we include bond stretching and angle bending (see Section 2.2.4). Part of the energy of the signal is used by intramolecular interactions. It is absorbed by the bonds and used for molecular reorientation [101] and creating an extended hydrogen bond network [102, 103] and relaxation [104, 105]. Additionally, it is consumed by intermolecular interactions such as rotational, vibrational, and translational motion [106].

All these change in the intermolecular interactions might affect the density of the water and therefore the sound velocity. This relation is written as:

$$c = \sqrt{\frac{K_s}{\rho}}, \tag{3.1}$$

where c is the sound velocity, K_s is the modulus of bulk elasticity for liquids, ρ is the density. The change in density of the water and the sound velocity alter the intensity such as:

$$I = 2\pi^2\nu^2\delta^2\rho c, \tag{3.2}$$

where I is the intensity, ν is the frequency of the sound, δ is the amplitude of the particle displacement.

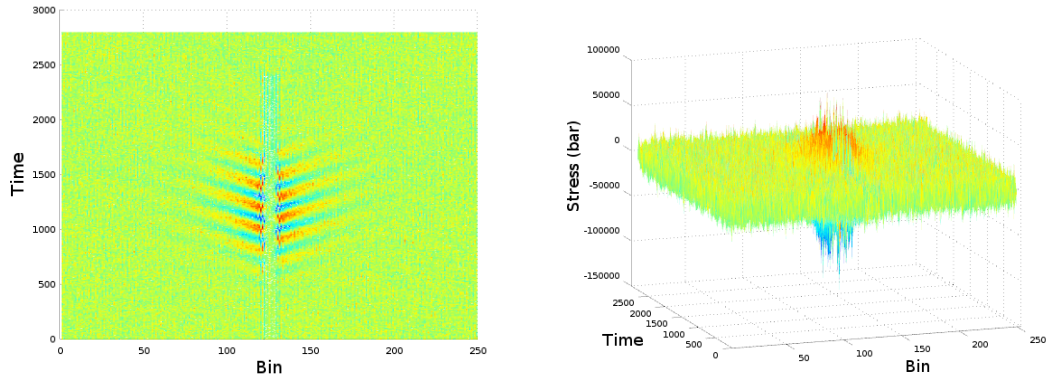

(a) **(b)**

Figure 3.2: Stress profile of the simulation systems with TIP4P/2005f potential. Variables used are frequency $f = 500$ GHz, Gaussian width $\sigma = 3000$ fs and amplitude $A_0 = 1$Å.

3.2 Spectral analysis

Following stress analysis, we will examine the spectral analysis of the results obtained from the simulations with mW and TIP4P/2005f potentials. In order to analyse the attenuation and the content of the signal, we applied Fast Fourier Transform on the stress results. Following FFT, we obtained the frequency power spectrum as it is explained in Section 2.5.

3.2.1 Spectral analysis of the simulations with mW potentials

Figure 3.3 provides the power spectrum of the signal, where the frequency is 750 GHz, amplitude is 1 Å and the signal width is 3000 Å. X axis shows the frequency decomposition of the signal and Y axis gives the power of the frequencies along the distance from the source of the signal. Each curve corresponds to each of the bins which were allocated as in Section 2.4 and visualized in Figure 3.1. For the spectral analysis, the results are rescaled by dividing the magnitude by 10^{10} in order to visualise more clearly.

From the Figure 3.3c we can see our signal at the fundamental frequency 750 GHz and its attenuation with distance. We marked the peak's borders to be able to calculate the area of the peaks. This will be examined further in the next Section 3.3. At frequency 1500 GHz (Figure 3.3d), whose value is the twice as the fundamental frequency, we observe a second harmonic generated by nonlinearity. For the mW simulations with the amplitude 1 Å, we detected second harmonic for all cases. Also for the cases for mW simulations with the amplitude 0.5 Å, second harmonics appear after the case with 500 GHz. From these observations, we can confirm that increase of frequency and amplitude induce the nonlinearity. It has been reported that the second harmonic might be useful to obtain some characteristics of the material since it depends on the pressure-density relation of the material [107]. However, in our study, we will dismiss the second harmonics. We will only analyse the fundamental frequency to calculate the attenuation, while keeping in mind that whatever causes the second harmonic might be the same for fast attenuation.

At low frequency region (Figure 3.3a) of the power spectrum, we can see sharply decaying peaks which arise from the noise. The magnitude of the peak increases with the increase of the frequency of the signal. Possible sources for this peak might be Brownian noise and flicker noise. Brownian noise is caused by the

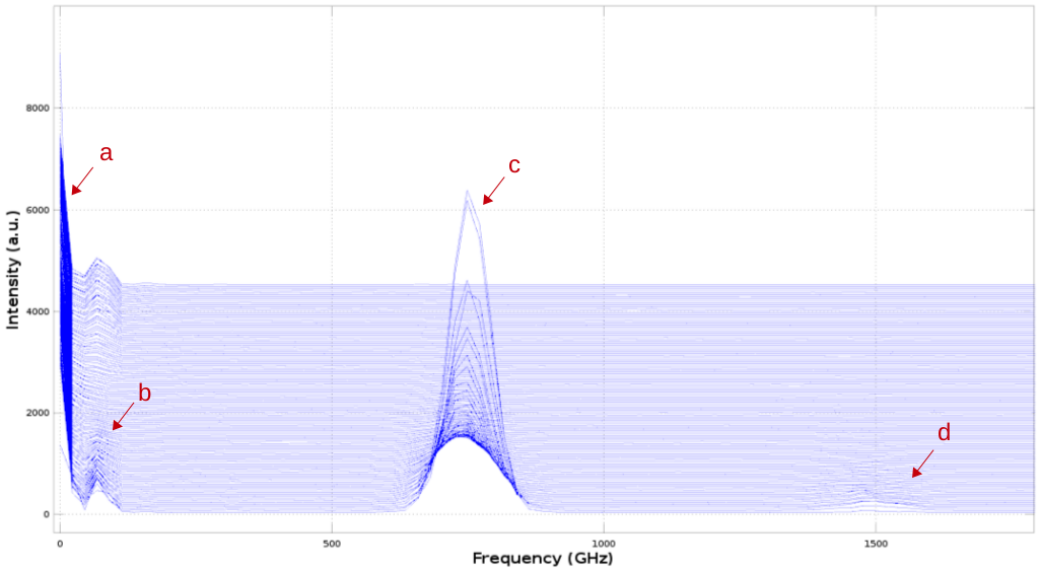

Figure 3.3: Power spectrum of mW simulations

Brownian motion of the molecules and can be calculated as the integration of the white noise. We also observe the white noise as small fluctuation along the spectrum due to the thermal noise. In addition flicker noise can be another contribution for this noise peak. Even though it has been observed mostly for the electronic devices, it has been also detected for various natural systems [108].

Beside of the noise peaks at the low frequency region, we see an indication for acoustic stream at the 0 frequency. Acoustic wave propagation with high amplitude at the non-linear regime generates an acoustic stream. It is produced by the gradients in momentum flux caused by the high attenuation of the acoustic wave [109, 110]. Generated acoustic stream is a time independent flow (DC flow) [111], whose shear stress is a function of shear rate at that instant. Since the flow does not move with the wavelike oscillatory motion, its frequency is 0.

What is interesting about the spectrum is that we see an unexpected peak at the frequency 67 GHz (Figure 3.3b). Closer inspection of the peak shows that it attenuates completely around the half way from the signal source to the simulation box boundary and reappears again till the boundary. We observe this peak in all

mW simulations at the same frequency. Unfortunately, we do not know how to interpret this peak.

3.2.2 Spectral analysis of the simulations with TIP4P/2005f potentials

Figure 3.4 provides the power spectrum of the signal, where the frequency is 750 GHz, amplitude is 1 Å and the signal width is 3000 Å.

From the Figure 3.4b we can observe the fundamental frequency at 750 GHz and its attenuation during the propagation along distance. Similar to the mW case, at the freqeuncy 1500 GHz (Figure 3.4c), we observe the second harmonic which was caused by nonlinearity. Moreover, noise at low frequencies is detected, however, due to the rescaling, it has not been seen easily at the power spectrum. In contrast to mW (Figure 3.3b), we did not observe a peak at 67 GHz. However, at that region, we see irregular peaks (Figure 3.4a). They can be interpreted as noise, however, they are more frequent than the thermal noise peaks, which are observed along the spectrum.

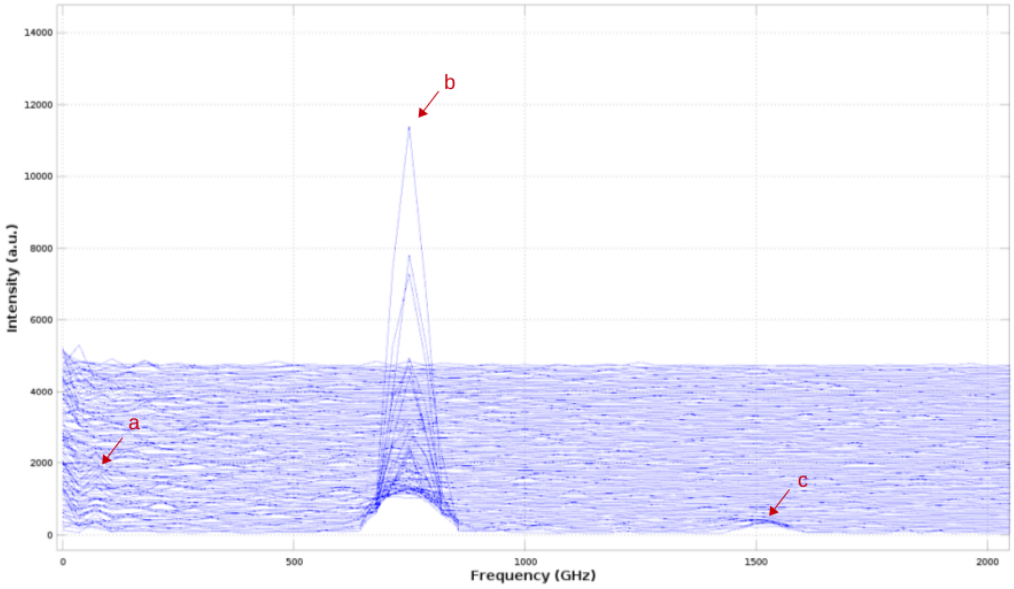

Figure 3.4: Power spectrum of TIP4P/2005f simulations

3.3 Acoustic attenuation analysis

Having analysed the FFT results, we will continue with the attenuation evaluation. We are interested in the power of each bin and how it changes with distance. In order to obtain the power of the peak from the fundamental frequency, with the best accuracy, we could integrate the area under the curve, however we chose to approximate the integral using the trapezoidal method. For the integration, we determined the borders of the peaks from FFT results, Figure 3.3 and Figure 3.4. We observed that the peaks got wider and possess Gaussian shape away from the source due to the attenuation and the tails of the peaks altered. This behaviour has been also observed during the experiments [43, 112] . Since their area is relatively small compare to the first peak, we decided to calculate the integral of all peaks with the first peak's borders. To increase the accuracies further, we computed the integration for both sides of the fixed atom in the simulation box and averaged them.

For each amplitude, we analysed several frequencies as given in Simulated System Details (Section 2.3). This analysis includes fitting data into

$$y = ae^{-bx} + c \tag{3.3}$$

which, as described in Section 3.3, is how attenuation behaves.

For curve fitting, we decided to exclude some outlying data both in the mW and TIP4P/2005f results, since they alter the best fit for the attenuation part dramatically. We showed the excluded data with a cut-off point in the graphs. In the following section, we will present the figures, showing the obtained results of the simulations of the mW and TIP4P/2005f potentials.

3.3.1 Acoustic attenuation analysis of the simulations with mW potentials

For the mW simulation results, we decided to exclude the long distance tail which was shown with cut-off point. We believe that the bumps that we observe at the frequency 125 GHz and 250 GHz (see Figures 3.5a, 3.5b, 3.6a, 3.6b, 3.7a and 3.7b) are due to the same reason as bumps which was previously mentioned in Sections 3.1.1 and 3.2.1, because of the periodic boundary condition and a possible induced stream. Even though, the bump does not show up in the attenuation graph of other higher frequency cases, we preferred to apply the cut-off on all mW simulation results, in order to make the comparison of the attenuation coefficient safe. On the other hand, in the stress plot and FFT analysis, bump appears in all cases. One possible implication of this might be that the incoming wave caused by periodic boundary or created stream interferes with our sound signal at high frequency, and this causes loss of the signal.

When we exclude the tail parts, in figures 3.5, 3.6, 3.7, we can observe that the attenuation follows an exponential function (see Equation 1.8).

In the following figures, we can see how the intensity behaves for each of the frequency. When the frequency increases, the intensity also increases as expected. The intensity also increases with the increase of the amplitude of the signal (see Figures 3.5, 3.6, 3.7)

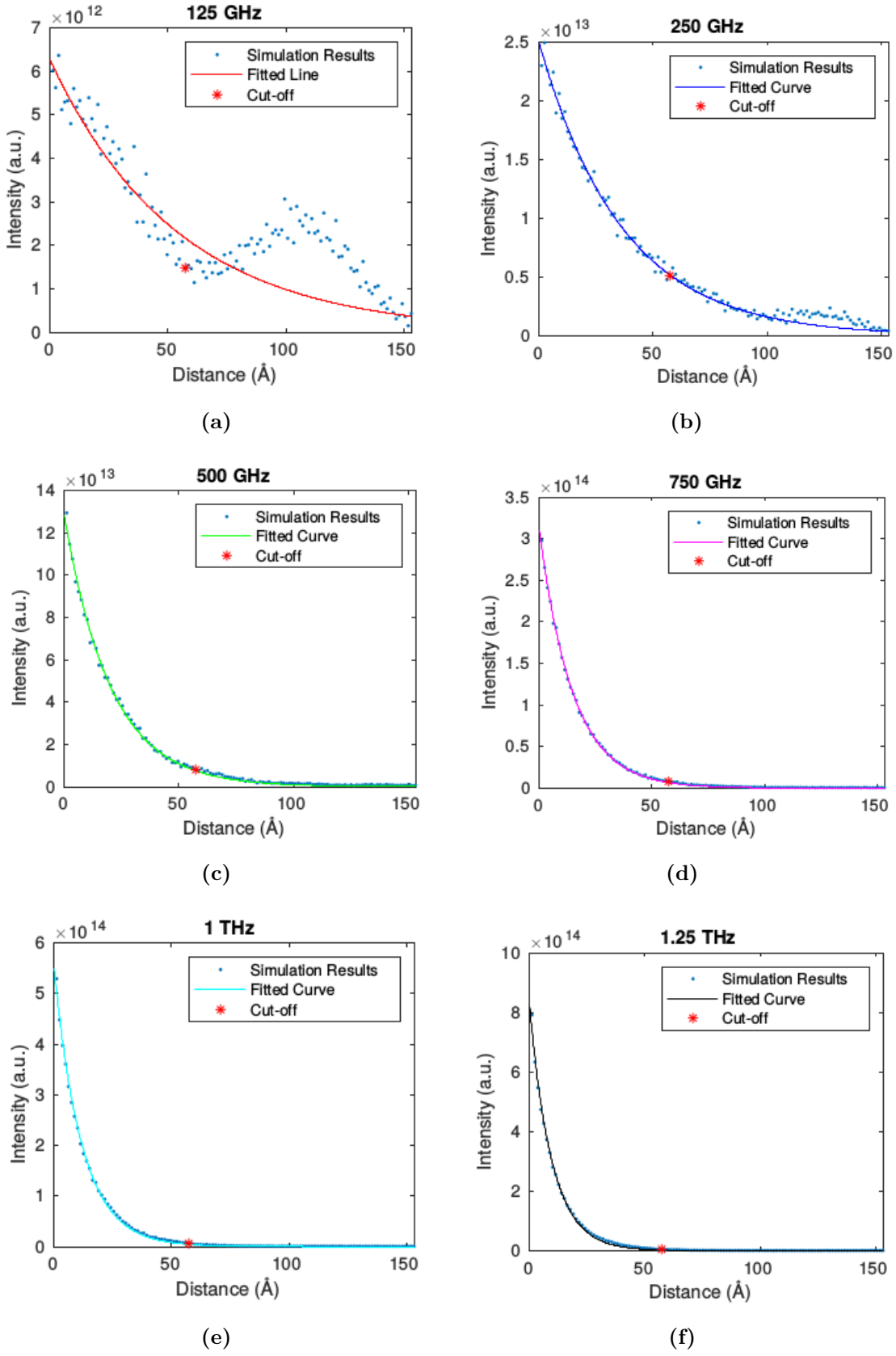

Figure 3.5: Attenuation graphs of mW simulations. Variables used are amplitude $A_0 = 0.25$ Å , Gaussian width $\sigma = 3000$Å, at the frequency a)125 GHz, b) 250 GHz, c) 500 GHz, d) 750 GHz, e)1 THz, f) 1.25 THz.

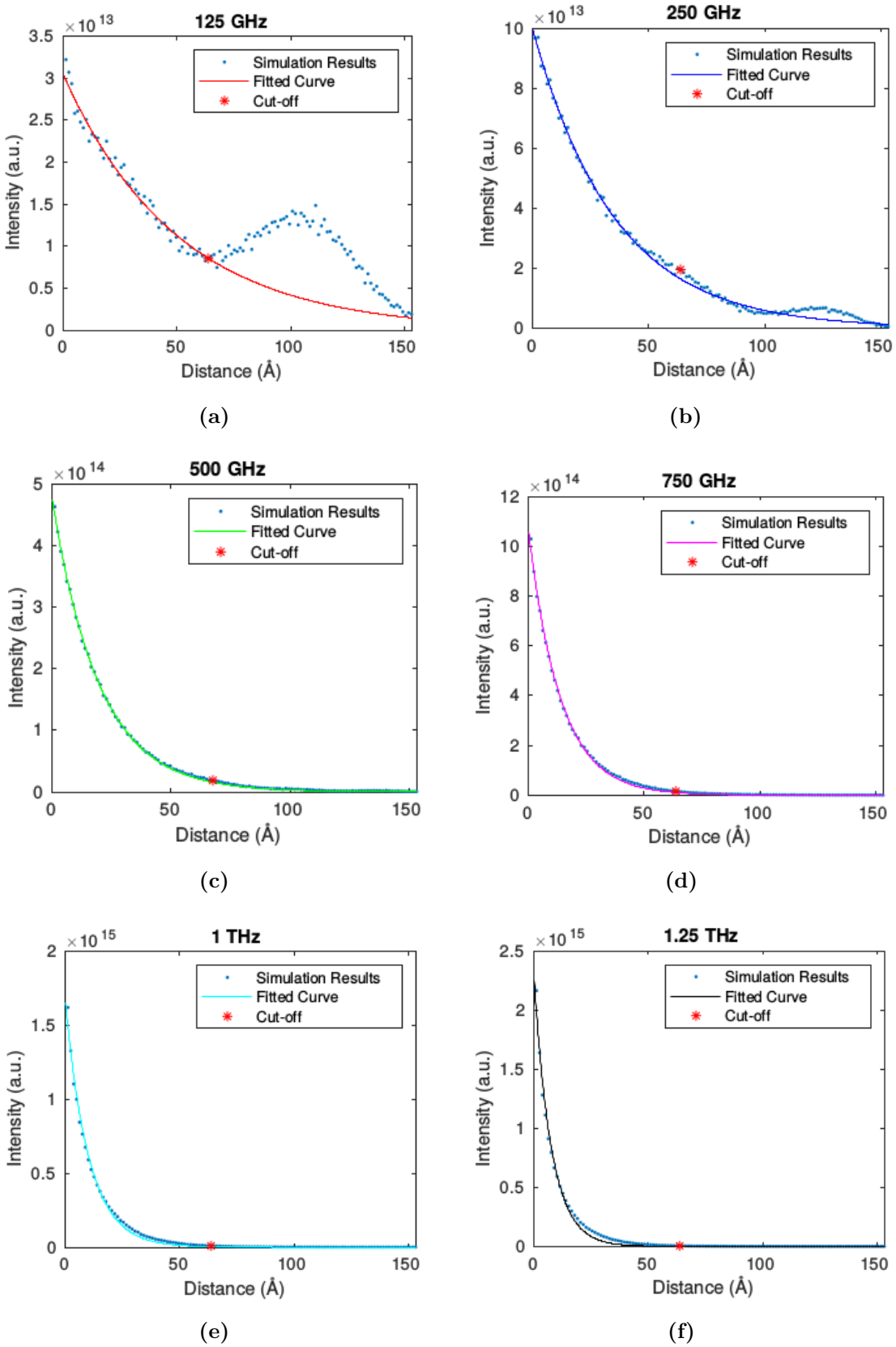

Figure 3.6: Attenuation graphs of mW simulations. Variables used are amplitude $A_0 = 0.5$ Å , Gaussian width $\sigma = 3000$Å, at the frequency a)125 GHz, b) 250 GHz, c) 500 GHz, d) 750 GHz, e)1 THz, f) 1.25 THz.

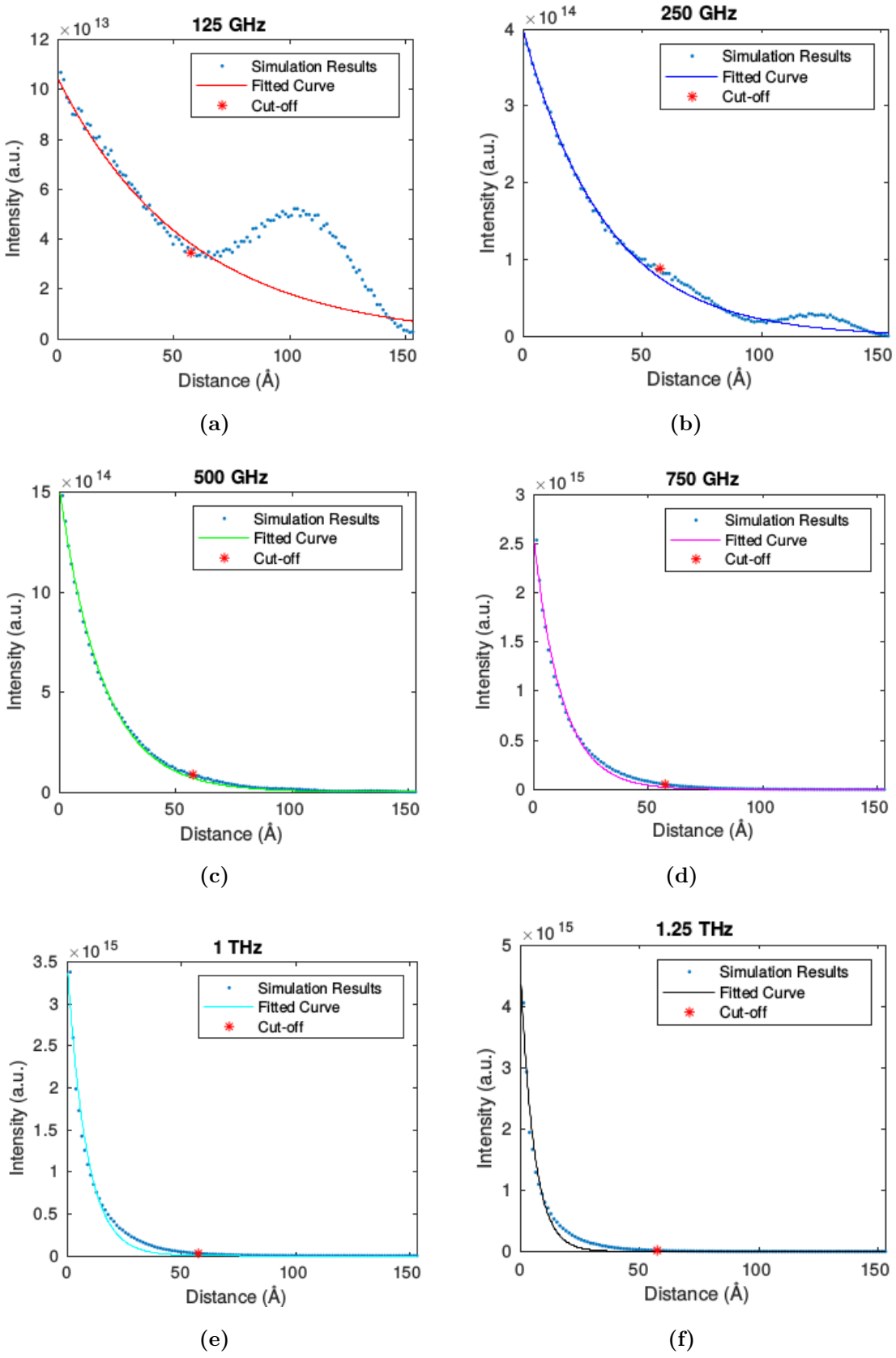

Figure 3.7: Attenuation graphs of mW simulations. Variables used are amplitude $A_0 = 1$ Å , Gaussian width $\sigma = 3000$Å, at the frequency a)125 GHz, b) 250 GHz, c) 500 GHz, d) 750 GHz, e)1 THz, f) 1.25 THz.

3.3.2 Acoustic attenuation analysis of the simulations with TIP4P/2005f potential

In theory, we would expect an exponential decreasing curve, however, we had an unexpected sharp decline in the first interval of the TIP4P/2005f simulation results. We had to discard the first 5 data points, which affect the best-fit line severely. We suspected that these data might be an artifact of the simulation. Another explanation might be structural change of water, related to the manifestation of Frenkel line model as explained in Section 1.2. If there is any structural change, the signal passing from amorphous to liquid might attenuate sharply due to the interfacial resistance [113] between two structures. This would clarify the interesting behaviour of the data.

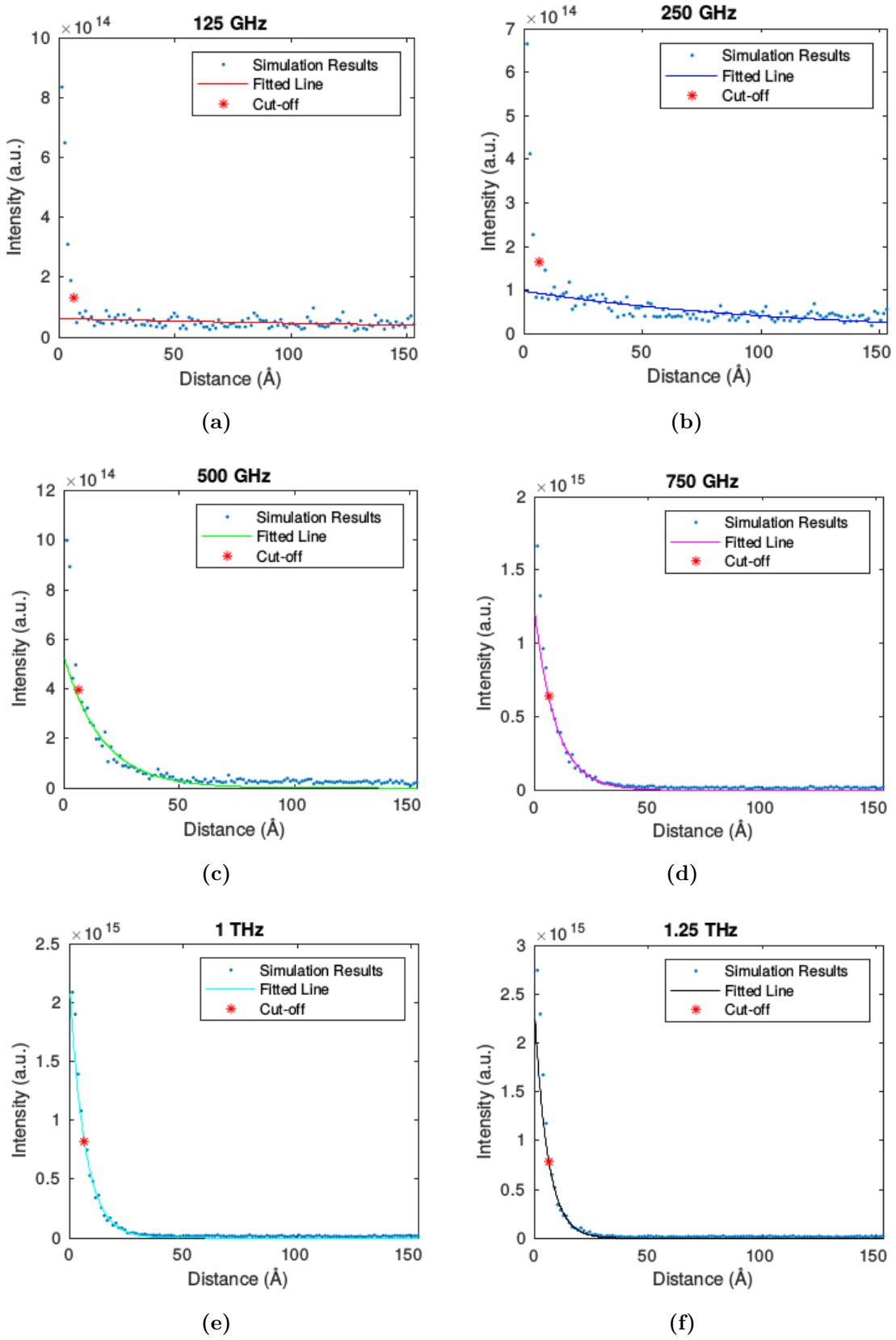

Figure 3.8: Attenuation graphs of TIP4P/2005f simulations. Variables used are amplitude $A_0 = 0.5$ Å , Gaussian width $\sigma = 3000$Å, at the frequency a)125 GHz, b) 250 GHz, c) 500 GHz, d) 750 GHz, e)1 THz, f) 1.25 THz.

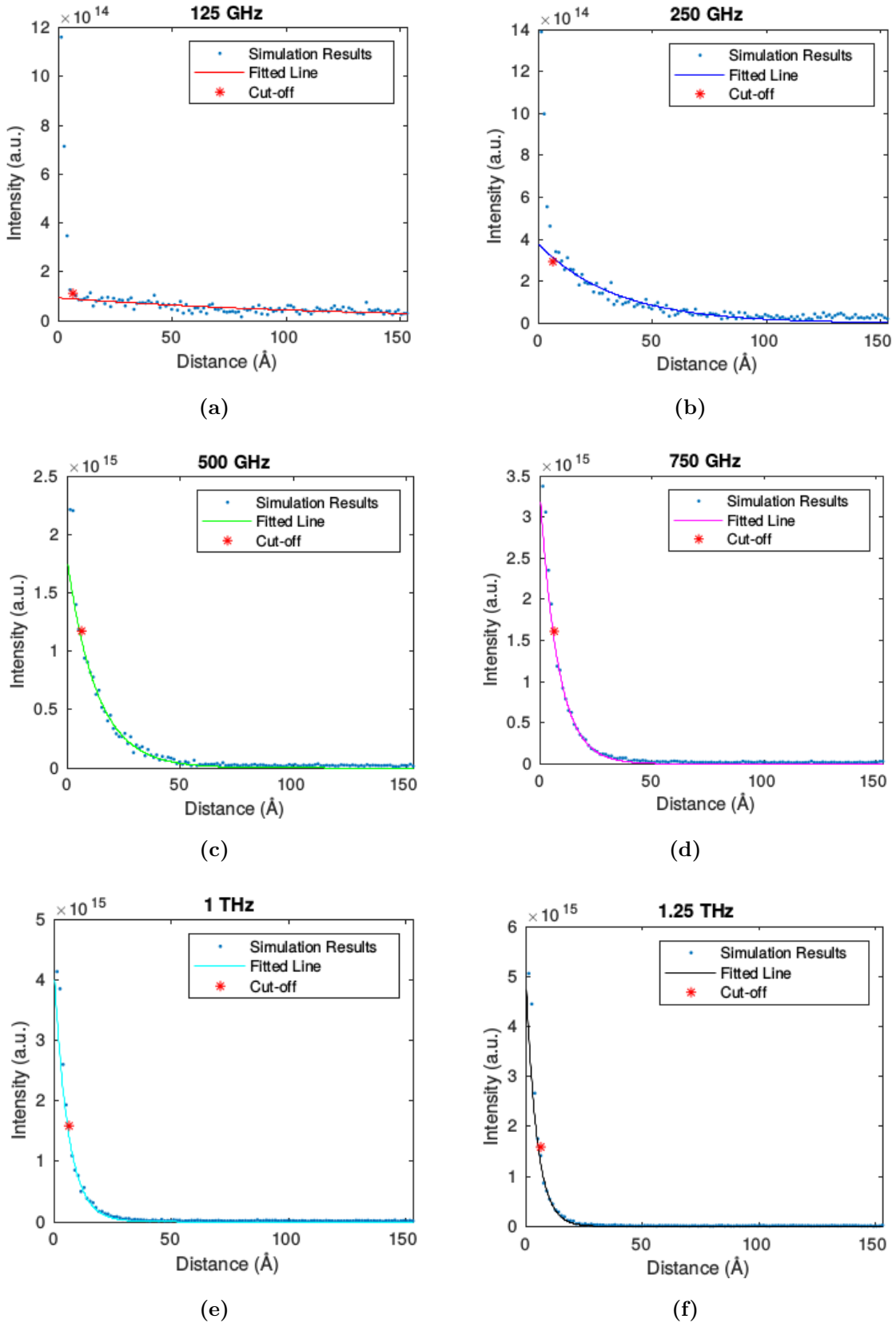

Figure 3.9: Attenuation graphs of TIP4P/2005f simulations. Variables used are amplitude $A_0 = 1$ Å , Gaussian width $\sigma = 3000$Å, at the frequency a)125 GHz, b) 250 GHz, c) 500 GHz, d) 750 GHz, e)1 THz, f) 1.25 THz.

3.4 Attenuation coefficient analysis

In this section we present the obtained attenuation coefficients with their corresponding error bars. We calculated the attenuation coefficients by taking the slope of each attenuation graph presented in the previous section (based on the exponential decay law (see Equation 1.8).)

According to the Stoke's Law Equation 1.7, we should observe a quadratic relationship between frequency and attenuation coefficient. However, we can not clearly tell so by looking at the graphs. We can observe that the attenuation grows monotonically, as the frequency increases.

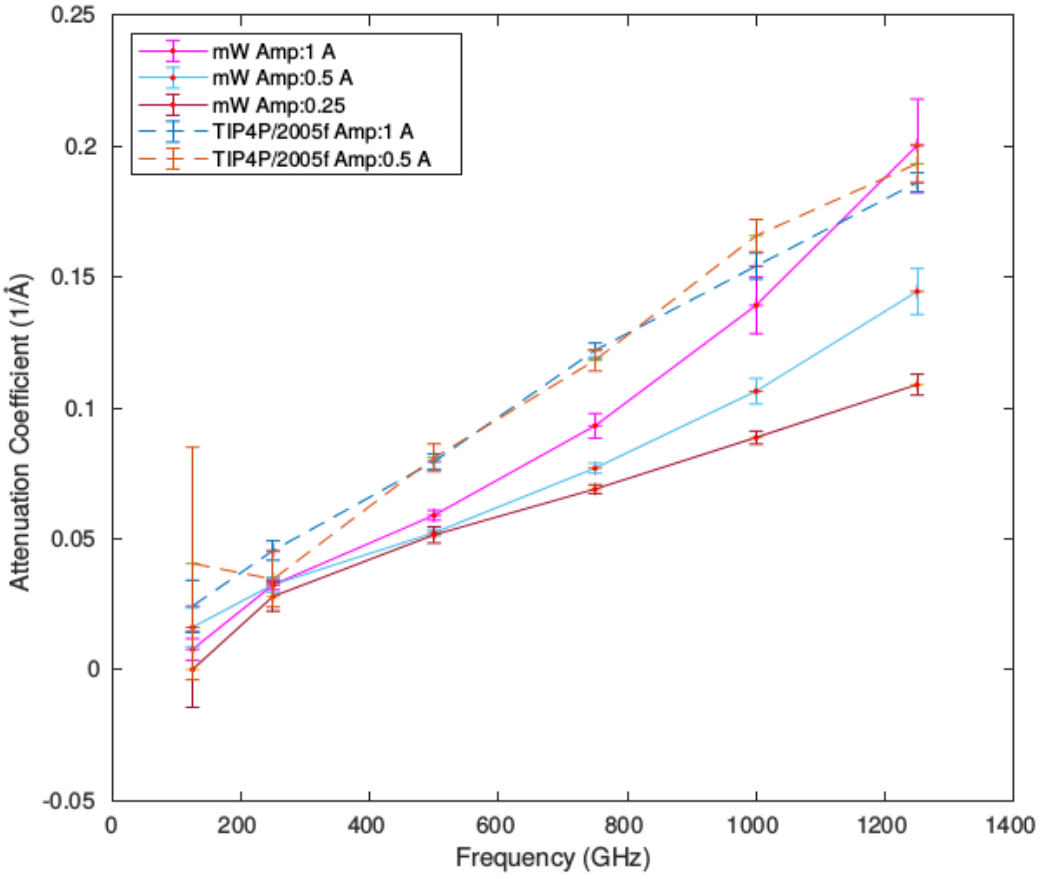

Figure 3.10: Attenuation coefficients obtained from the simulation results.

A possible explanation might be, that the period of the wave applied is significantly smaller than the relaxation time, which seems to support the ideas brought

forward by Frenkel [13].

Increasing the amplitude does not seem to have much of an effect in simulations with TIP4P/2005f potential. But we should keep in mind that we excluded the first part, which might have a useful information hidden there. On the other hand, in simulations with mW, the increase of the amplitude causes an increase in the attenuation rate.

It is also interesting that TIP4P/2005f simulations seems to have a higher coefficient than mW ones, no matter the amplitude. This might be caused by the inter- and intramolecular interactions as mentioned in Section 3.3. We would like to compare the results with experimental data, however the results we found target a frequency range much different than ours (see Figure 1.8).

4. Conclusion

The purpose of this study was to determine the attenuation coefficient of hypersound in water through Molecular Dynamics. We have shown that the attenuation at high frequency is high, as can be seen in Figure 3.10. This causes a big loss of the sound intensity. As a result, the sound signal might diminish before it reaches the sample. Therefore it is important to determine a signal with a maximum frequency, which can travel the water medium between the lens and the sample as well as provides a good resolution.

A possible solution for the high attenuation at the hypersound, might be adding electrolytes into the water. It has been shown that electrolytes reduce the sound absorption [114, 115]. Another solution might be improving a measurement setup, where the coupling medium thickness is at the nanometer range, since the amplitude attenuates in couple of Å at high frequencies.

We also compared two water potentials by simulating water with a coarse grain model, mW, and a more detailed one, TIP4P/2005f. When comparing the two water potentials, we observed that the power of the signal differs, which might be related to the difference in the structure of the potential. We suspect that, at high frequency, a stream arises which might be an obstacle for an acoustic microscope.

We plan to use a bigger simulation box to investigate the possible effects of the periodic boundary condition. We observed a lack of experimental data with the set-up we simulated, and thus would like to obtain it to validate the results of our

simulations. Further work needs to be done to establish whether the high frequency induced structural changes are responsible for the high attenuation. This might be answered through methods studying structure order parameter, radial distribution function, hydrogen bond length, H-O-H angle analysis, sound velocity and particle tracking.

5. Acknowledgements

I would like to express my deep gratitude to my supervisor Antti Kuronen for his guidance and encouragement. Thank you for all the things you taught me and answering my questions patiently with a kind smile. After discussing problems with you, they always looked smaller and solvable. Also, thank you for trusting me, giving me the freedom and time to explore questions on my own.

I would like to acknowledge Kai Nordlund as the second reader of this thesis. Also, thank you for suggesting a study plan which opened new doors for me. I would also like to thank Ari Salmi for introducing me to nanoacoustics and his catching enthusiasm during the courses. My grateful thanks are also extended to Simo Huotari for introducing me to the Solid State course, which encouraged me to continue studying Physics.

I also wish to thank to CSC – IT Center for Science, Finland, and Accelerator Laboratory for the facilities and resources.

I am truly thankful to all my colleagues and friends from the accelerator lab, my second home. Thank you Jyri for your help in academic related questions, discussions and laughs; Alvaro for sharing the longing for the south and your unconditional support despite of the distance; Elnaz for our sisterhood; Jesper for laughing at my bad jokes gently and Henrique for your loud laughs and always positive attitude; Junlei for the fruitful discussions about the work. My friends outside of the lab but from the Kumpula Campus, Santeri, Chema, Anshuman, and Llorenç, without you,

Finnish winters would be even darker. Thank you for your amazing friendship.

I would also like to extend my thanks to University of Helsinki and Finland for the opportunity to study. It was a big challenge for me to live alone here and start studying physics. I experienced a different education system, in which I had more self confidence and pushed my limits more. Through these years, I grew up, matured, met lovely people, and witnessed the extremes and beauties of nature. I am grateful for all of these.

I would also like to thank Ozric Tentacles, Hidria Spacefolk and Faithless for their company through this work with their perpetual sound.

Finally, I wish to thank my family for their love, support and encouragement throughout my life. I always find peace in your big hug.

Bibliography

1 Richard P Feynman. There's plenty of room at the bottom: An invitation to enter a new field of physics. In *Handbook of Nanoscience, Engineering, and Technology, Third Edition*, pages 26–35. CRC Press, 2012.

2 Chris Toumey. Plenty of room, plenty of history. *Nature nanotechnology*, 4(12):783, 2009.

3 Gerd Binnig, Heinrich Rohrer, Ch Gerber, and Edmund Weibel. Surface studies by scanning tunneling microscopy. *Physical review letters*, 49(1):57, 1982.

4 Gerd Binnig, Calvin F Quate, and Ch Gerber. Atomic force microscope. *Physical review letters*, 56(9):930, 1986.

5 Martin Maldovan. Sound and heat revolutions in phononics. *Nature*, 503(7475):209, 2013.

6 Sebastian Volz, Jose Ordonez-Miranda, Andrey Shchepetov, Mika Prunnila, Jouni Ahopelto, Thomas Pezeril, Gwenaelle Vaudel, Vitaly Gusev, Pascal Ruello, Eva M Weig, et al. Nanophononics: state of the art and perspectives. *The European Physical Journal B*, 89(1):15, 2016.

7 Jaeho Lee, Woochul Lee, Geoff Wehmeyer, Scott Dhuey, Deirdre L Olynick, Stefano Cabrini, Chris Dames, Jeffrey J Urban, and Peidong Yang. Investiga-

tion of phonon coherence and backscattering using silicon nanomeshes. *Nature communications*, 8:14054, 2017.

8 Huanyang Chen and CT Chan. Acoustic cloaking in three dimensions using acoustic metamaterials. *Applied physics letters*, 91(18):183518, 2007.

9 John R Hook and Henry Edgar Hall. Solid state physics (the manchester physics series), 1991.

10 Anthony Frederic John Levi. *Essential Classical Mechanics for Device Physics*. Morgan & Claypool Publishers, 2016.

11 Dima Bolmatov, Dmitry Zav'yalov, Mikhail Zhernenkov, Edvard T Musaev, and Yong Q Cai. Unified phonon-based approach to the thermodynamics of solid, liquid and gas states. *Annals of Physics*, 363:221–242, 2015.

12 Dima Bolmatov, VV Brazhkin, and Kostya Trachenko. The phonon theory of liquid thermodynamics. *Scientific reports*, 2:421, 2012.

13 J Frenkel. Kinetic theory of liquids,(1955). *NY Dover Publ*, 8:143.

14 K Trachenko and VV Brazhkin. Collective modes and thermodynamics of the liquid state. *Reports on Progress in Physics*, 79(1):016502, 2015.

15 Dima Bolmatov, Mikhail Zhernenkov, Dmitry Zav'yalov, Stanislav Stoupin, Alessandro Cunsolo, and Yong Q Cai. Thermally triggered phononic gaps in liquids at thz scale. *Scientific reports*, 6:19469, 2016.

16 E Pontecorvo, M Krisch, A Cunsolo, G Monaco, A Mermet, R Verbeni, F Sette, and G Ruocco. High-frequency longitudinal and transverse dynamics in water. *Physical Review E*, 71(1):011501, 2005.

17 G Ruocco and F Sette. The history of the" fast sound" in liquid water. *Condensed Matter Physics*, 2008.

18 Aneesur Rahman and Frank H Stillinger. Propagation of sound in water. a molecular-dynamics study. *Physical Review A*, 10(1):368, 1974.

19 Karl F Herzfeld and Theodore A Litovitz. *Absorption and dispersion of ultrasonic waves*, volume 7. Academic Press, 2013.

20 A Akhieser. On the absorption of sound in solids. *J. Phys.(Ussr)*, 1:277, 1939.

21 Calvin F Quate, Abdullah Atalar, and HK Wickramasinghe. Acoustic microscopy with mechanical scanning—a review. *Proceedings of the IEEE*, 67(8):1092–1114, 1979.

22 George Gabriel Stokes. On the theories of the internal friction of fluids in motion, and of the equilibrium and motion of elastic solids. *Transactions of the Cambridge Philosophical Society*, 8, 1880.

23 T Pritz. Frequency power law of material damping. *Applied Acoustics*, 65(11):1027–1036, 2004.

24 E Kinsler Lawrence, R Frey Austin, B Coppens Alan, and V Sanders James. Fundamentals of acoustics. *New yorks: John wileys*, page 151, 2000.

25 Jacek Jarzynski. Mechanisms of sound attenuation in materials. *Sound and vibration damping with polymers*, pages 167–207, 1990.

26 Pascal Ruello and Vitalyi E Gusev. Physical mechanisms of coherent acoustic phonons generation by ultrafast laser action. *Ultrasonics*, 56:21–35, 2015.

27 Osamu Matsuda, Maria Cristina Larciprete, Roberto Li Voti, and Oliver B Wright. Fundamentals of picosecond laser ultrasonics. *Ultrasonics*, 56:3–20, 2015.

28 JL Hostetler, AN Smith, and PM Norris. Thin-film thermal conductivity and thickness measurements using picosecond ultrasonics. *Microscale Thermophysical Engineering*, 1(3):237–244, 1997.

29 Oliver B Wright, Bernard Perrin, O Matsuda, and VE Gusev. Ultrafast carrier diffusion in gallium arsenide probed with picosecond acoustic pulses. *Physical Review B*, 64(8):081202, 2001.

30 Guray Tas and Humphrey J Maris. Electron diffusion in metals studied by picosecond ultrasonics. *Physical Review B*, 49(21):15046, 1994.

31 PA Mante, JF Robillard, and A Devos. Complete thin film mechanical characterization using picosecond ultrasonics and nanostructured transducers: Experimental demonstration on sio 2. *Applied Physics Letters*, 93(7):071909, 2008.

32 LL Chapelon, J Vitiello, D Neira, J Torres, JC Royer, D Barbier, F Naudin, G Tas, P Mukundhan, and J Clerico. Measuring the young's modulus of ultralow-k materials with the non destructive picosecond ultrasonic method. *Microelectronic engineering*, 83(11-12):2346–2350, 2006.

33 G Andrew Antonelli, Humphrey J Maris, Sandra G Malhotra, and James ME Harper. Picosecond ultrasonics study of the vibrational modes of a nanostructure. *Journal of applied physics*, 91(5):3261–3267, 2002.

34 Floyd Dunn and William J Fry. Ultrasonic absorption microscope. *The Journal of the Acoustical Society of America*, 31(5):632–633, 1959.

35 S Che, PR Guduru, AV Nurmikko, and HJ Maris. A scanning acoustic microscope based on picosecond ultrasonics. *Ultrasonics*, 56:153–159, 2015.

36 Daniel Veira Canle, Tuukka Kekkonen, Joni Mäkinen, Tuomas Puranen, Heikki J Nieminen, Antti Kuronen, Sami Franssila, Tapio Kotiaho, Ari Salmi,

and Edward Hæggström. Practical realization of a sub-$\lambda/2$ acoustic jet. *Scientific reports*, 9(1):5189, 2019.

37 Manfred Radmacher, Monika Fritz, Claudia M Kacher, Jason P Cleveland, and Paul K Hansma. Measuring the viscoelastic properties of human platelets with the atomic force microscope, 1996.

38 RA Lewis, CJ Hall, Alan P Hufton, S Evans, RH Menk, F Arfelli, L Rigon, G Tromba, DR Dance, IO Ellis, et al. X-ray refraction effects: application to the imaging of biological tissues. *The British journal of radiology*, 76(905):301–308, 2003.

39 Anthony S Stender, Kyle Marchuk, Chang Liu, Suzanne Sander, Matthew W Meyer, Emily A Smith, Bhanu Neupane, Gufeng Wang, Junjie Li, Ji-Xin Cheng, et al. Single cell optical imaging and spectroscopy. *Chemical reviews*, 113(4):2469–2527, 2013.

40 Richard Neutze, Remco Wouts, David van der Spoel, Edgar Weckert, and Janos Hajdu. Potential for biomolecular imaging with femtosecond x-ray pulses. *Nature*, 406(6797):752, 2000.

41 Clément Rossignol, Nikolay Chigarev, M Ducousso, B Audoin, Guillaume Forget, F Guillemot, and MC Durrieu. In vitro picosecond ultrasonics in a single cell. *Applied Physics Letters*, 93(12):123901, 2008.

42 Srirang Manohar and Daniel Razansky. Photoacoustics: a historical review. *Advances in optics and photonics*, 8(4):586–617, 2016.

43 TJ Grimsley, F Yang, S Che, GA Antonelli, HJ Maris, and AV Nurmikko. Ultrafast opto-acoustics applied to the study of material nanostructures. In *Journal of Physics: Conference Series*, volume 278, page 012037. IOP Publishing, 2011.

44 Tribikram Kundu, Joon-Pyo Lee, Christopher Blase, and Jürgen Bereiter-Hahn. Acoustic microscope lens modeling and its application in determining biological cell properties from single-and multi-layered cell models. *The Journal of the Acoustical Society of America*, 120(3):1646–1654, 2006.

45 Jacques Rouch, CC Lai, and Sow-Hsin Chen. High frequency sound velocity and sound absorption in supercooled water and the thermodynamic singularity at 228° k. *The Journal of Chemical Physics*, 66(11):5031–5034, 1977.

46 AI Erokhin. Water structure and supergigahertz phonons. *Journal of Russian Laser Research*, 23(4):369–380, 2002.

47 F Sette, G Ruocco, M Krisch, C Masciovecchio, R Verbeni, and U Bergmann. Transition from normal to fast sound in liquid water. *Physical review letters*, 77(1):83, 1996.

48 Thomas Dehoux, Maroun Abi Ghanem, Omar F Zouani, Mathieu Ducousso, Nikolay Chigarev, Clément Rossignol, Nicolas Tsapis, Marie-Christine Durrieu, and Bertrand Audoin. Probing single-cell mechanics with picosecond ultrasonics. *Ultrasonics*, 56:160–171, 2015.

49 Ning Wang, Jessica D Tytell, and Donald E Ingber. Mechanotransduction at a distance: mechanically coupling the extracellular matrix with the nucleus. *Nature reviews Molecular cell biology*, 10(1):75, 2009.

50 Claudia Tanja Mierke. The fundamental role of mechanical properties in the progression of cancer disease and inflammation. *Reports on Progress in Physics*, 77(7):076602, 2014.

51 Paul A Janmey and R Tyler Miller. Mechanisms of mechanical signaling in development and disease. *J Cell Sci*, 124(1):9–18, 2011.

52 Geoffrey M Cooper, Robert E Hausman, and Robert E Hausman. *The cell: a molecular approach*, volume 10. ASM press Washington, DC, 2000.

53 Young Min Rhee, Eric J Sorin, Guha Jayachandran, Erik Lindahl, and Vijay S Pande. Simulations of the role of water in the protein-folding mechanism. *Proceedings of the National Academy of Sciences*, 101(17):6456–6461, 2004.

54 John E Ladbury. Just add water! the effect of water on the specificity of protein-ligand binding sites and its potential application to drug design. *Chemistry & biology*, 3(12):973–980, 1996.

55 Yaakov Levy and José N Onuchic. Water mediation in protein folding and molecular recognition. *Annu. Rev. Biophys. Biomol. Struct.*, 35:389–415, 2006.

56 I Shvab and Richard J Sadus. Atomistic water models: Aqueous thermodynamic properties from ambient to supercritical conditions. *Fluid Phase Equilibria*, 407:7–30, 2016.

57 Thorsten Bartels-Rausch, Vance Bergeron, Julyan HE Cartwright, Rafael Escribano, John L Finney, Hinrich Grothe, Pedro J Gutiérrez, Jari Haapala, Werner F Kuhs, Jan BC Pettersson, et al. Ice structures, patterns, and processes: A view across the icefields. *Reviews of Modern Physics*, 84(2):885, 2012.

58 Olgierd Cecil Zienkiewicz, Robert Leroy Taylor, Perumal Nithiarasu, and JZ Zhu. *The finite element method*, volume 3. McGraw-hill London, 1977.

59 COMSOL Multiphysics. Introduction to comsol multiphysics®. *COMSOL Multiphysics, Burlington, MA, accessed Feb*, 9:2018, 1998.

60 Normand M Laurendeau. *Statistical thermodynamics: fundamentals and applications*. Cambridge University Press, 2005.

61 LH Thompson and LK Doraiswamy. Sonochemistry: science and engineering. *Industrial & Engineering Chemistry Research*, 38(4):1215–1249, 1999.

62 Daniel Schanz, Burkhard Metten, Thomas Kurz, and Werner Lauterborn. Molecular dynamics simulations of cavitation bubble collapse and sonoluminescence. *New Journal of Physics*, 14(11):113019, 2012.

63 Guancong Ma and Ping Sheng. Acoustic metamaterials: From local resonances to broad horizons. *Science advances*, 2(2):e1501595, 2016.

64 Igor Ostrovskii, Nataliya Ostrovskaya, Oleg Korotchenkov, and James Reidy. Radiation defects manipulation by ultrasound in ionic crystals. *IEEE transactions on nuclear science*, 52(6):3068–3073, 2005.

65 Daan Frenkel and Berend Smit. *Understanding molecular simulation: from algorithms to applications*, volume 1. Elsevier, 2001.

66 Berni J Alder and T E Wainwright. Studies in molecular dynamics. i. general method. *The Journal of Chemical Physics*, 31(2):459–466, 1959.

67 Ludwig Boltzmann. *Vorlesungen über Gastheorie: 2. Teil*. BoD–Books on Demand, 2017.

68 Max Born and Robert Oppenheimer. Zur quantentheorie der molekeln. *Annalen der Physik*, 389(20):457–484, 1927.

69 Antti Kuronen. Lecture notes in computational nanoscience, September 2015.

70 Steve Plimpton. Fast parallel algorithms for short-range molecular dynamics. *Journal of computational physics*, 117(1):1–19, 1995.

71 William C Swope, Hans C Andersen, Peter H Berens, and Kent R Wilson. A computer simulation method for the calculation of equilibrium constants for the

formation of physical clusters of molecules: Application to small water clusters. *The Journal of Chemical Physics*, 76(1):637–649, 1982.

72 Loup Verlet. Computer" experiments" on classical fluids. i. thermodynamical properties of lennard-jones molecules. *Physical review*, 159(1):98, 1967.

73 Michael P Allen and Dominic J Tildesley. *Computer simulation of liquids*. Oxford university press, 2017.

74 Andrew R Leach. *Molecular modelling: principles and applications*. Pearson education, 2001.

75 Roger W Hockney and James W Eastwood. *Computer simulation using particles*. crc Press, 1988.

76 Charles William Gear. The numerical integration of ordinary differential equations. *Mathematics of Computation*, 21(98):146–156, 1967.

77 Miguel A González and José LF Abascal. A flexible model for water based on tip4p/2005. *The Journal of chemical physics*, 135(22):224516, 2011.

78 Shuichi Nosé. A unified formulation of the constant temperature molecular dynamics methods. *The Journal of chemical physics*, 81(1):511–519, 1984.

79 William G Hoover. Canonical dynamics: equilibrium phase-space distributions. *Physical review A*, 31(3):1695, 1985.

80 Mark Tuckerman. *Statistical mechanics: theory and molecular simulation*. Oxford university press, 2010.

81 Herman JC Berendsen, JPM van Postma, Wilfred F van Gunsteren, ARHJ DiNola, and JR Haak. Molecular dynamics with coupling to an external bath. *The Journal of chemical physics*, 81(8):3684–3690, 1984.

82 Hans C Andersen. Molecular dynamics simulations at constant pressure and/or temperature. *The Journal of chemical physics*, 72(4):2384–2393, 1980.

83 Kevin R Hadley and Clare McCabe. Coarse-grained molecular models of water: a review. *Molecular simulation*, 38(8-9):671–681, 2012.

84 G Wilse Robinson, S Singh, Sheng-Bai Zhu, and Myron W Evans. *Water in biology, chemistry and physics: experimental overviews and computational methodologies*, volume 9. World Scientific, 1996.

85 Bertrand Guillot. A reappraisal of what we have learnt during three decades of computer simulations on water. *Journal of Molecular Liquids*, 101(1-3):219–260, 2002.

86 Carlos Vega, Jose LF Abascal, MM Conde, and JL Aragones. What ice can teach us about water interactions: a critical comparison of the performance of different water models. *Faraday discussions*, 141:251–276, 2009.

87 William L Jorgensen, Jayaraman Chandrasekhar, Jeffry D Madura, Roger W Impey, and Michael L Klein. Comparison of simple potential functions for simulating liquid water. *The Journal of chemical physics*, 79(2):926–935, 1983.

88 Michael W Mahoney and William L Jorgensen. A five-site model for liquid water and the reproduction of the density anomaly by rigid, nonpolarizable potential functions. *The Journal of Chemical Physics*, 112(20):8910–8922, 2000.

89 Herman JC Berendsen, James PM Postma, Wilfred F van Gunsteren, and Jan Hermans. Interaction models for water in relation to protein hydration. In *Intermolecular forces*, pages 331–342. Springer, 1981.

90 Ariel A Chialvo and Peter T Cummings. Engineering a simple polarizable model for the molecular simulation of water applicable over wide ranges of state conditions. *The Journal of chemical physics*, 105(18):8274–8281, 1996.

91 Janusz Bytnar, Anna Kucaba-Pietal, and Zbigniew Walenta. Influence of molecular models of water on computer simulations of water nanoflows. In *2008 International Multiconference on Computer Science and Information Technology*, pages 269–275. IEEE, 2008.

92 Mingsen Deng and Hujun Shen. Coarse-grained model for water involving a virtual site. *The Journal of Physical Chemistry B*, 120(4):733–739, 2016.

93 Valeria Molinero and Emily B Moore. Water modeled as an intermediate element between carbon and silicon. *The Journal of Physical Chemistry B*, 113(13):4008–4016, 2008.

94 Jose LF Abascal and Carlos Vega. A general purpose model for the condensed phases of water: Tip4p/2005. *The Journal of chemical physics*, 123(23):234505, 2005.

95 Carlos Vega and Jose LF Abascal. Simulating water with rigid non-polarizable models: a general perspective. *Physical Chemistry Chemical Physics*, 13(44):19663–19688, 2011.

96 Philip M Morse. Diatomic molecules according to the wave mechanics. ii. vibrational levels. *Physical Review*, 34(1):57, 1929.

97 Alan Hinchliffe. *Molecular modelling for beginners*. John Wiley & Sons, 2005.

98 Aidan P Thompson, Steven J Plimpton, and William Mattson. General formulation of pressure and stress tensor for arbitrary many-body interaction potentials under periodic boundary conditions. *The Journal of chemical physics*, 131(15):154107, 2009.

99 Joseph Fourier. *Theorie analytique de la chaleur, par M. Fourier*. Chez Firmin Didot, père et fils, 1822.

100 Peter Welch. The use of fast fourier transform for the estimation of power spectra: a method based on time averaging over short, modified periodograms. *IEEE Transactions on audio and electroacoustics*, 15(2):70–73, 1967.

101 Damien Laage and James T Hynes. A molecular jump mechanism of water reorientation. *Science*, 311(5762):832–835, 2006.

102 Daniel C Elton and Marivi Fernández-Serra. The hydrogen-bond network of water supports propagating optical phonon-like modes. *Nature communications*, 7:10193, 2016.

103 Stefano Bellissima, Simone De Panfilis, Ubaldo Bafile, Alessandro Cunsolo, Miguel Angel González, Eleonora Guarini, and Ferdinando Formisano. The hydrogen-bond collective dynamics in liquid methanol. *Scientific reports*, 6:39533, 2016.

104 DP Nandedkar. Analysis of dipole relaxation time for water molecules at temperature of 293 0 k. *Phys. J*, 2:15–22, 2016.

105 Jakob Petersen, Klaus B Møller, Rossend Rey, and James T Hynes. Ultrafast librational relaxation of h2o in liquid water. *The Journal of Physical Chemistry B*, 117(16):4541–4552, 2012.

106 Pankaj Kr Mishra, Vincent Bettaque, Oriol Vendrell, Robin Santra, and Ralph Welsch. Prospects of using high-intensity thz pulses to induce ultrafast temperature-jumps in liquid water. *The Journal of Physical Chemistry A*, 122(23):5211–5222, 2018.

107 Xiufen Gong, Dong Zhang, Jiehui Liu, Huanlei Wang, Yongsheng Yan, and Xiaochen Xu. Study of acoustic nonlinearity parameter imaging methods in reflection mode for biological tissues. *The Journal of the Acoustical Society of America*, 116(3):1819–1825, 2004.

108 Eiji Yamamoto, Takuma Akimoto, Masato Yasui, and Kenji Yasuoka. Origin of 1/f noise in hydration dynamics on lipid membrane surfaces. *Scientific reports*, 5:8876, 2015.

109 JE Piercy and J Lamb. Acoustic streaming in liquids. *Proc. R. Soc. Lond. A*, 226(1164):43–50, 1954.

110 James Lighthill. Acoustic streaming. *Journal of sound and vibration*, 61(3):391–418, 1978.

111 Junru Wu. Acoustic streaming and its applications. *Fluids*, 3(4):108, 2018.

112 F Yang, T Atay, CH Dang, TJ Grimsley, S Che, J Ma, Q Zhang, AV Nurmikko, and HJ Maris. Study of phonon propagation in water using picosecond ultrasonics. In *Journal of Physics: Conference Series*, volume 92, page 012024. IOP Publishing, 2007.

113 LJ Challis. Kapitza resistance and acoustic transmission across boundaries at high frequencies. *Journal of Physics C: Solid State Physics*, 7(3):481, 1974.

114 TO Woodruff and H Ehrenreich. Absorption of sound in insulators. *Physical Review*, 123(5):1553, 1961.

115 B Cros, V Gigot, and G Despaux. Study of the efficiency of coupling fluids for acoustic microscopy. *Applied surface science*, 119(3-4):242–252, 1997.